AERODYNAMIC CHARACTERISTICS OF JOUKOWSKY AIRFOILS IN A NONUNIFORM STRONG SHEAR FLOW

By

SUMITABH BISWAS

DEPARTMENT OF AERONAUTICAL ENGINEERING

INDIAN INSTITUTE OF TECHNOLOGY KANPUR

SEPTEMBER, 1976

AERODYNAMIC CHARACTERISTICS OF JOUKOWSKY AIRFOILS IN A NONUNIFORM STRONG SHEAR FLOW

A Thesis Submitted
in Partial Fulfilment of the Requirements
for the Degree of
MASTER OF TECHNOLOGY

By
SUMITABH BISWAS

to the

DEPARTMENT OF AERONAUTICAL ENGINEERING
INDIAN INSTITUTE OF TECHNOLOGY KANPUR
SEPTEMBER, 1976

AE-1976-M-BIS-AER

CERTIFICATE

Certified that this work entitled "AERODYNAMIC CHARACTERISTICS OF JOUKOWSKY AIRFOILS IN A NONUNIFORM STRONG SHEAR FLOW" by Sumitabh Biswas has been carried out under my supervision and that this has not been submitted elsewhere for a degree.

A. K. Gupta

(A.K. Gupta)
Assistant Professor
Department of Aeronautical Engineering
Indian Institute of Technology Kanpur.

ACKNOWLEDGEMENT

I am very grateful to Dr. A.K. Gupta, who guided and encouraged me at all stages of the work. He has been a real source of inspiration and it was a pleasure to work under him.

I want to express my thanks to Mr. R. Krishnamurthy who took a lot of pains during the workshop job.

I also want to thank Mr. K.S. Muddappa and Mr. P.R. Choudhuri, who helped me during the Experimental Program.

ABSTRACT

An experimental studyof a cambered Joukowsky airfoil (chord 15 cms, thickness 15%, camber 10%) and a symmetric Joukowsky airfoil (chord 15 cms, thickness 15%) has been carried out in nonuniform strong shear flow. A shear screen was designed and fabricated to generate unonuniform strong shear flow and a new model incidence system was designed and fabricated to measure the geometrical angle of attack of the airfoils with an accuracy of 1/10th of a degree. The pressure distributions over the airfoils have been measured to compute the aerodynamic coefficients C_L, C_M and C_D for various angles of attack and at different vertical locations to observe the effects of the interactions of stream shear, camber, thickness and vertical location on the airfoil characteristics. The present work shows that maximum lift obtained both for the symmetric airfoil and the cambered airfoil decreases considerably when nonuniform strong shear is introduced, although as the airfoil is mounted further and further away from the flow centreline the maximum lift obtained for both airfoils increases. The improvement is more for vertical locations below the flow centreline compared to vertical locations above the flow centreline. The variation of C_M with angle of attack and different vertical locations is presented and discussed.

CONTENTS

LIST OF SYMBOLS

$2a$	Test Section Width = 12"
$2b$	Test Section Height = 48"
c	Airfoil Chord = 6"
C_c	Chordwise Force Coefficient
C_{DP}	Pressure /Drag Coefficient Based on the Airfoil Midchord Dynamic Head
C_L	Lift Coefficient, Based on the Airfoil Midchord Dynamic Head
$C_{M_{L.E.}}$	Pitching Moment Coefficient at the Leading Edge Based on Midchord Dynamic Pressure (positive, nose up)
C_N	Normal Force Coefficient
C_p	Nonuniform Flow Pressure Coefficient, Based on $\bar{U}$ corresponding to Airfoil Mid Chord Vertical Location, $\frac{p_s - p}{\frac{1}{2}\rho \bar{U}^2}$
d	Diameter of Rod
$\overline{h}$	Maximum Height of the Airfoil Camber Line for the Cambered Airfoil
K	Shear Parameter ..... Eq. 1.1
K_o	Screen Resistence Coefficient .... Eq. 1.7
p_s	Static Pressure on the Airfoil Surface
p	Free Stream Static Pressure
q	Shear Parameter ..... Eq. 1.4
s	Spacing between the Rods
t	Maximum Thickness of the Airfoil
U_o	Uniform Free Stream Velocity Upstream of Screen
$\bar{U}$	Local Mean Velocity
U_c	Velocity of Free Stream at the Centre of the Horizontal Pitot Rake when it is mounted at a vertical location on the vertical pitot rake.
U_{rms}	Root Mean Square Velocity in fps.
X,Y,Z	Cartesian Coordinates.
y	Vertical Location of the Airfoil Midchord Measured from the Middle of the Test Section Height

z Distance of a Pitot Static Probe on the Horizontal Pitot Rake From the Centre of the Horizontal Pitot Rake

α Angle of Attack

α_0 Zero Lift Angle of Attack

β Defined in Eq. 1.8

σ Solidity of the Screen, d/s

τ Thickness Ratio = t/c

ρ Density of Air

Subscripts

u Upper Surface

l Lower Surface

LIFT OF FIGURES

Figure

20. $C_{M_{L.E.}}$ vs α in shear flow for the vertical locations y/b = $\pm$ 0.041(y=$\pm$1") for the symmetric airfoil

21. $C_{M_{L.E.}}$ vs α in shear flow for the vertical locations y/b = $\pm$ 0.083 (y = $\pm$ 2") for the symmetric airfoil

22. $C_{M_{L.E.}}$ vs α in shear flow for the vertical locations y/b = $\pm$ 0.167 (y = $\pm$ 4") for the symmetric airfoil

23. $C_{M_{L.E.}}$ vs α (uniform flow), $C_{M_{L.E.}}$ vs α (shear flow, vertical location y = 0) for the cambered airfoil

24. $C_{M_{L.E.}}$ vs α in shear flow for the vertical location y/b = $\pm$ 0.041 (y = $\pm$ 1") for the cambered airfoil

25. $C_{M_{L.E.}}$ vs α in shear flow for the vertical locations y/b = $\pm$ 0.083 (y = $\pm$ 2") for the cambered airfoil

26. $C_{M_{L.E.}}$ vs α in shear flow for the vertical locations y/b = $\pm$ 0.167 (y = $\pm$ 4") for the cambered airfoil

27. C_{DP} vs α (Uniform flow), C_{DP} vs α (shear flow, vertical location y = o) for the symmetric airfoil

28. C_{DP} vs α (Uniform flow), C_{DP} vs α (shear flow, vertical location y/= 0) for the cambered airfoil

29. $\pm C_p$ vs x/c, in uniform flow and shear flow (vertical location y = o) for the symmetric airfoil

30. $-C_p$ vs x/c, in shear flow for the vertical locations y/b = $\pm$ 0.041 (y = $\pm$ 1") for the symmetric airfoil

31. $-C_p$ vs x/c, in shear flow for the vertical locations y/b = $\pm$ 0.167 (y = $\pm$ 4") for the symmetric airfoil

32. $-C_p$ vs x/c, in uniform flow and shear flow (vertical location y = 0) for the cambered airfoil

33. $-C_p$ vs x/c, in shear flow for the vertical locations y/b = $\pm$ 0.041 (y = $\pm$ 1 ") for the cambered airfoil

34. $-C_p$ vs x/c, in shear flow for the vertical locations y/b = $\pm$ 0.167 (y = $\pm$ 4") for the cambered airfoil

LIST OF PHOTOGRAPHS

Photograph

CHAPTER 1

INTRODUCTION

The majority of aerodynamic problems are concerned with the determination of forces on bodies immersed in a uniform stream. But there are situations in which the flow approaching the body cannot be considered uniform. In other words it has velocity gradients or shear. For example, the flow in propeller or jet slip-streams, flow in the wakes of bodies, and in Boundary layers fall into this category of shear flows. In the case of a propeller aircraft where part of the wing is submerged in the slipstream, the local lift coefficient on this part of the wing may differ from that on the rest of the wing, changing the spanwise lift distribution accordingly.

Recently attention has been focused on shear flows because of the importance of rotor or propeller slipstream interaction with the wings of V/STOL aircraft. Both theoretical and experimental investigations on airfoils have been carried out in various types of shear flows where the shear exists in a plane perpendicular to the span of the wing. Existence of strong gradients of the longitudinal velocity in the slipstream seems to change the airfoil characteristics considerably. An understanding of the maximum lift and stalling behavior of airfoils in nonuniform shear flows should enable the airplane designer to take maximum advantage of this if possible. This will be particularly useful in the field of V/STOL aircraft with highly flapped wings immersed in a highly sheared slipstream.

1.1 Review of the Previous Work

a. Airfoils in Uniform Shear Flow.

In one of the earliest investigations Tsien[1] (1943) considered a symmetric Joukowsky airfoil in an infinite inviscid stream with a uniform shear K, defined as

$$U = U_o \left(1 + \frac{Ky}{c}\right) \qquad (1.1)^*$$

---

* See list of symbols for definitions.

An exact solution for the aerodynamic forces was obtained predicting an increase in the lift coefficient due to interaction of thickness and shear. Tsien's theory for a symmetric Joukowsky airfoil in a 2-dimensional uniformly sheared stream (i.e. with constant shear throughout the flow) was extended by Sowyrda[2] (1958) to the case of a cambered Joukowsky airfoil, mainly due to his interest in the deflected shear slipstream over highly flapped wing configurationsof V/STOL aircraft. His results for the lift coefficient and the pitching moment coefficient to the first order in the thickness τ and camberh/c are

$$C_L \approx \left(1 + \tau + \frac{\tau K^2}{32} \right) 2\pi\alpha + 2\pi\left(\frac{\tau K}{4} + \frac{2\bar{h}}{c}\left(1 + \frac{K^2}{32} \right)\right) \qquad (1.2)$$

$$C_{M_{c/2}} \approx \left(1 + \tau + \frac{\tau K^2}{16} \right)\frac{\pi}{2}\alpha + \frac{\tau \pi K}{64} \qquad (1.3)$$

where $\bar{h}$ is the maximum height of the airfoil camber line. If in Eq. (1.2) $\bar{h}$ is put equal to zero, the value of C_L given by Tsien's theory is obtained.

An experimental study was also undertaken by Vidal[4,5] in which measurements were made on a symmetric 2-dimensional Joukowsky airfoil. A Joukowsky airfoil was chosen so that the results could be compared to the predictions of the theories available at the time. One particularly notable result was obtained when the airfoil was immeresed in a nonuniformly sheared flow similar to a section through a propeller slipstream. It was found that the location of the airfoil in this flow had a marked effect on both the maximum lift available and on the stalling characteristics of the airfoil. Indeed it was observed t that a small change in the vertical location of the airfoil relative to the flow centreline, say, of approximately one airfoil thickness, produced about a 100% change in maximum lift available. The theories available at the time did not provide a satisfactory explanation for the flow mechanism involved in producing such a marked effect.

b. Airfoils in Nonuniform Shear Flow.

Jones[3] (1957) investigated the effect of nonuniform flow on airfoil characteristics with a parabolic velocity distribution given by

$$U = U_1 \left(1 + 8q \left(\frac{y}{c} \right)^2 \right) \qquad (1.4)$$

His results for C_L and $C_{M_{c/2}}$ to the first order in angle of attack α and shear parameter q are given by

$$C_L = 2\pi \left(\left(1 + 1.11q \right)\alpha + \frac{2\bar{h}}{c} \right) \qquad (1.5)$$

$$C_{M_{c/2}} \approx \frac{\pi}{2}\alpha \left(1 + .866q \right) \qquad (1.6)$$

Ludwig and Erickson[6] (1971) at the Cornell Aeronautical Laboratory (now CALSPAN Corporation) carried out a systematic study of the aerodynamic characteristics of symmetrical airfoils in shear flows. They developed a theoretical and experimental program to investigate the aerodynamics of an airfoil in a 2-dimensional nonuniformly sheared slipstream. A mathematical model was developed to predict airfoil pressure distributions in such a slipstream and was used successfully for slipstreams with moderate shear. Pressure distributions over a wide angle of attack range were measured experimentally on an airfoil at each of seven different locations in a highly sheared 2-dimensional slipstream. Pressure distributions were obtained on the airfoil both at a location slightly above the flow centreline and also at a location slightly below the flow centreline. These effects indicated that the large effects on stalling characteristics were due to differences in the upper surface pressure distributions. The pressure distributions were affected by the free stream shear. Moreover, in the data obtained for airfoils located near the flow centreline, the differences in the lift appreared to have been caused primarily by differences in the stagnation pressure of the streamline which intersected the airfoil. This stagnation pressure was a function not only of airfoil location relative to the slipstream, but also of the angle of attack of the airfoil.

Vidal et al[4] (1960) made experimental measurements by simulating a 2-dimensional nonuniform slipstream in a wind tunnel and carried out tests on a 17% thick symmetrical Joukowsky airfoil. It was reported that the maximum lift available changed markedly when the airfoil was positioned slightly below or above the flow centreline. Vidal[5] (1962) also found that the stalling characteristics of airfoil in shear flows depended upon the product of the local shear and its derivative, which when negative delayed stalling, and promoted it when positive.

Gupta and Sharma[16,17] (1974) carried out an experimental study of a 2-dimensional cambered Joukowsky airfoil (chord 15 cms, thickness 15% and camber 10%)in nonuniformly sheared flow. The pressure distribution over the airfoil was measured to compute the aerodynamic coefficients, C_L and C_M for various angles of attack and at different vertical locations to observe the effect of the interaction of stream shear, camber and thickness on the airfoil characteristics. As shown in earlier works it was noticed the maximum lift on a 2-dimensional symmetrical Joukowsky airfoil increased when it was located slightly below the flow centreline. The results obtained for symmetrical airfoil showed good agreement with previous work. In addition the results for a cambered Joukowsky airfoil immersed in nonuniform shear flow showed an increase in the lift/in not agreement with the theoretical predictions. The value of the shear parameter q in their experiments was 0.0476.

c. Production of Nonuniform Shear Flow.

The production of nonuniform shear flow is very essential for an experimental study of airfoils in such flows. This type of flow can be generated in a wind tunnel, by incorporating variable losses in the test section. These losses can be produced by placing an array of spanwise rods/wires with variable spacings.

When a turbulent stream of fluid passes through a wire gauze, it becomes less turbulent and the steady disturbances are reduced in intensity.

The gauze offerss a resistance to the component of flow normal to its plane. If a pressure difference p_1-p_2 is required to drive fluid of density ρ, through a wire gauze at a velocity U, the drag coefficient K_o (also called screen resistance coefficient), is given by

$$K_o = \frac{p_1 - p_2}{\frac{1}{2}\rho U^2} \qquad (1.7)$$

Taylor and Batchelor[7] (1949) solved the problem of flow through a gauze and found that the longitudinal velocity was altered in the ration

$$\frac{u_2}{u_1} = \frac{1 + \beta - \beta K_o}{1 + \beta + K_o} \qquad (1.8)$$

where $\beta = 1.1.\ (1+K_o)^{-\frac{1}{2}}$, and the flow patterns far downstream were not the same as those for upstream.

Owen and Zienkiewicz[8] (1957) found a linear relationship between downstream velocity distribution and K_o, the screen resistance coefficient, distribution across a grid of horizontal wires. By inserting such grid in the test section of a wind-tunnel, a weak uniform shear flow was obtained. Elders[9] (1958)obtained similar results. McCarthy[10] (1964) obtained a nonlinear relation between downstream velocity distribution and K_o for 3-dimensional highly nonuniform shear flows. Vidal et al[4] (1960) extended Owen and Zienkiewicz's method to produce a nihighly nonuniform shear stream. For experimental results, empirical formulae with trials and errors alongwiththe theory were used. The velocity profiles of Vidal et al were in good agreement with the theory.

Kotnasky[11] (1966) made use of a honey comb structure for generating nonuniform flows. The cellular structure of honey comb eliminates most of the support and structural problems associated with shear screens of rods and wires. Because of the built-in straightness, the flow downstream was relatively homogeneous. Livesay and Laws[12] (1973) have given a method of generating axisymmetric gauze screens required to produce desired velocity profiles by developing and adding corrections to Elder's theory.

1.2 The Present Work

The present work is experimental and is an extension of the work of Sharma and Gupta[17] and Sharma (1974)[16]. In the present experiments a 2-dimensional cambered Joukowsky airfoil and a symmetrical Joukowsky airfoil were used. Both the airfoils have chords of 15 cm and 15% thickness. The cambered airfoil had 10% camber. These were tested in a strong nonuniform shear flow to record the pressure distribution along the mid-span. The objective was to study the aerodynamic characteristics of cambered and symmetrical Joukowsky airfoil in strong nonuniform shear flow for different angles of attack and at different vertical locations.

A strong nonuniform shear flow similar to, but with a much higher value of the shear parameter ($q = .282$) than in ref. 17 was obtained by introducing variable losses in the wind tunnel test section with the help of a shear screen. The screen consisted of an array of rods arranged horizontally but much more closely packed than in ref. 17, so as to get a strong nonuniform shear flow.

In Gupta and Sharma's[17] (1974) work the mechanism for changing the angle of attack of an airfoil was to stop the tunnel and then move the airfoil mounting, noting the angle change through a pointer and an ordinary geometrical compass protactor. This was a very crude method and in any case the error introduced could be of the order of $1/2^{\circ}$.

We wanted to have a mechanism by which the airfoil could be rotated continuously even when the tunnel was running. So we designed and fabricated a completely new model incidence system which had an accuracy of 1/10th of a degree and using which the airfoil could be rotated continuously even when the tunnel was running but at the same time it was constrained from rotating due to the aerodynamic forces in the tunnel.

Lift, drag and pitching moment characteristics for each airfoil were computed from the pressure distribution recorded. An attempt to qualitatively

look at the stalling characteristics of the two airfoils was also made by means of pressure distribution and C_L Vs α curve.

CHAPTER 2

EXPERIMENTAL PROGRAM

The testing of 2-dimensional Joukowsky (cambered and symmetric) was carried out in a strong nonuniform shear flow, for various angles of attack and at different vertical locations. The strong nonuniform shear flow was produced by incorporating variable losses with the help of a screen consisting of an array of horizontal circular rods of varying diameters and spacings, and mounted in the test section 36" ahead of the airfoil. The airfoil was mounted on a model incidence system which permitted an independent change of the angle of attack and the vertical location.

2.1 Equipment

(i) Wind Tunnel.

The experiments were conducted in the 2-D test section of the 5-D low speed tunnel in the Aero Lab at IIT/Kanpur. This tunnel has a special feature that, with a common blower return section, two different test sections can be used one at a time. The 2-D test section with a contraction ratio of 9.0 has a cross section of 1'x4' and a length (distance between the contraction cone and the diffuser) of 5'-6". The maximum velocity attained with no model in it is 180fps and the turbulence level at this speed is 1.4%.

(ii) Airfoil Models.

Two Joukowsky airfoils (cambered and symmetrical) were used for testing. Both the airfoil models were 15% thick, having a chord of 15 cms and a span of 12 inches. These were manufactured in the Aero Workshop out of compressed seasoned wood. There were twenty five static pressure tappings along the midspan of the symmetrical airfoil as shown in Fig 1, and twenty three static pressure tappings as shown in Fig 2. The copper tubes of 1/16" diameter used as pressure leads from both the models were taken out from one side of the airfoil model through a hole of 1/2" diameter at the midchord. One mild steel tube of 3/4" outer diameter with outside threads was fixed

permanently for the model support as well as for taking the pressure leads to the multitube manometer. The pressure measurements at the trailing edge could be taken with the help of two static pressure probes, as it can be seen from the airfoil cross section (Figs. 1 & 2) that taking the pressure leads out of the trailing edge was not possible because of the thinness of the trailing edge.

(iii) Model Support.

Unlike the earlier work (Sharma[16] 1973, Gupta & Sharma[17] 1974) where a simple model support system was used, a device was designed and fabricated for manually changing the angle of attack of a 2-dimensional airfoil mounted in the tunnel when the tunnel was running.

Background.

The mechanism used previously to change the angle of attack of an airfoil was by loosening a nut to rotate the airfoil by hand and noting the angle change by means of a pointer and a geometrical compass protactor. This was a very crude method, and in any case, the error introduced could be easily of the order of $1/2^{\circ}$. Also we wanted to design a mechanism by which the airfoil could be rotated continuously and the readings could be observed easily with an accuracy better than $1/2^{\circ}$.

Technical Details.

We decided to achieve an accuracy of $1/10^{\circ}$. The set up had to be made in a way so that the airfoil could be rotated by means of a handle driven mechanism, but at the same time it would not rotate by itself because of aerodynamic forces on the airfoil in the tunnel. For this it became imperative to use a worm and worm wheel setu up. It was also decided to achieve a $1/10^{\circ}$ rotation of the airfoil through one revolution of the counter to be turned by handle. The worm and worm wheel were therefore expected to have a ratio of 1:3600. Since this would involve unmanageable sizes of the worm and worm wheel we decided to use two sets of worm and worm wheel, one giving a ratio

the worm wheel of the 1:30 set on the same axis as the worm for the 1:120 set and so both were fabricated out of one piece of brass together forming one piece.

As is clear from the Figs. 3 & 4 and the photograph of the device (photograph 1) it consists basically of these two sets of worm and worm wheel which are mounted on an aluminium base plate. There is a cylindrical shaft with a through and through hole through which the mild steel tube attached to the airfoil passes and is held rigidly to the device with the help of screws. The shaft itself passes through the aluminium worm wheel of the 1:120 set. The worm wheel is in contact with the brass worm to which is attached (in the same piece of metal) the worm wheel of the other set, which is engaged to the other worm. This is connected through a set of bevel gears to a handle and a five digit mechanical reversible counter. There is a pointer attached to the central shaft which moves on a 360° protactor. This protactor is mounted on an aluminium yoke which is fixed to the base plate and through which the cylindrical shaft passes. The mild steel tube fixed permanently to the airfoil and through which the copper tubes used as pressure leads come out is passed through the central shaft with the airfoil edge resting against the other surface of the base plate and the mild steel tube is held to the device with the help of screws for which holes have been drilled on the shaft side (photograph 2). There is another mild steel bracket fixed to the plate and the counter is mounted on this bracket. Holes were drilled at the edge of the base plate at 1" intervals so that the device could be used for stations above and below the centreline of the tunnel (photograph 3). One can read the number of rotations of the handle on the counter and for each rotation of the handle the pointer moves 1/10th of a degree on the protactor; i.e., it takes ten rotations of the handle to move the pointer by 1° on the protactor. Ball bearings have not been used in the design because the rate of rotations are fairly slow.

(iv) Screen for Nonuniform Strong Shear Flow.

A shear screen of aluminium frame was made for producing a nonuniform

strong shear flow. It consisted of aluminium rods of $\frac{1}{2}$" diameter and a few brass rods of $\frac{1}{4}$" diameter mounted in the aluminium frame. The locations of the centres of the rods have been shown in Fig. 5. The array of rods arranged horizontally was firmly secured in an aluminium frame of size 1' x 4' (photograph 4).

Before the aluminium screen was made a wooden screen was also made using wooden rods. But when it was mounted in the tunnel and tested it was found to be giving a strongly asymetric shear flow. This was due to the fact that the wooden rods could not be fixed very accurately at the desired locations resulting in gaps of varying sizes. So it was decided to get a metal screen made. The metal selected was aluminium due to its light weight.

The aluminium screen was placed in the test section 20 in. downstream of the contraction cone and the airfoil was placed 36 in downstream. This distance was the same as suggested by Ludwig & Erickson[6] (1971). The screen was held against four aluminium supports of L section which were firmly screwed to the tunnel walls (photgraph 5). The main criterion of the shear screen design was the proper distribution of the screen resistance coefficient K_o given by

$$K_o = \frac{p_1 - p_2}{\frac{1}{2}\rho U^2} \qquad (1.7)$$

where p_1 and p_2 are the static pressures upstream and downstream of the screen.

The distribution of the solidity over the range was determined by using one of the empirical relations:

$$K_o = \left(\frac{\sigma}{1-\sigma}\right)^2 \qquad (2.1)$$

$$K_o = \frac{\sigma - (2/3)\sigma^2}{(1-\sigma)^2} \qquad (2.2)$$

By choosing proper rod size, spacings could be found. This was the method adopted by Sharma[16] (1973). However we mainly used a qualitative criterion of providing more spacing in the larger velocity region to obtain the final distribution of rod spacings. Several iterations and tests were required for this purpose.

(v) Instrumentation and Accessories.

Hot Wire Anemometer.

A DISA, Model 55A01, constant temperature hot wire anemometer was used for the turbulence measurements. A single hot wire probe normal to the flow was traversed in the y direction from the centre of the tunnel test section at the point of airfoil midchord location. A Tektronix type 545 B oscilloscope was used for monitoring the hot wire signals.

Multitube Manometer.

The multitube manometer using water as the working fluid had a set of 50 tubes and could be inclined at any desired angle. However throughout the experiments we kept it positioned at 60° to the horizontal.

Pitot Static Tube.

A pitot static tube of diameter 3/8" was used to measure the total and static heads both infront of the shear screen and at the point where the airfoil was located. The tube was inserted in both places through holes made in the tunnel base.

Pitot Rakes.

A 40 tube vertical pitot rake was also used to measure the mean velocity profile. It was placed 36 in. downstream of the screen. A ten tube horizontal pitot rake was also used for 2-dimensionality boundary layer measurements. It was mounted on the vertical pitot rake at three locations and was used to measure spanwise velocity profiles.

Flow Angle Probe.

The flow angle was measured by means of a cylindrical probe of 1/8 in. diameter, and 12 in. in length, the axis of which was perpendicular and horizontal to the mean flow direction. Two pressure holes of 0.02 in. diameter were made 72° apart on the circular periphery in a plane about $\frac{1}{2}$ in. from sealed tip of the cylindrical probe, and the two leads from these pressure holes were taken out of the other tip to connect to a water multitube manometer. The other tip of the 1/8 in. diameter probe was keyed to a 4 in. dia-

meter disk marked on its periphery with protactor like graduations with a resolution of one degree. A pointer indicated amount of rotation in degrees of the cylindrical probe about its axis. The flow angle probe assembly was mounted on a tripod stand fitted with a rack and pinmion type vertical traverse arrangement. The cylindrical probe was inserted into the test section at the airfoil location vertical plane through a side panel which had 1/8 in. diameter holes spaced 1 in. apart vertically. The flow angle was measured by rotating the cylindrical probe about its axis until the same pressure from the 72° apart two pressure holes was measured on the manometer.

2.2 Procedure

The first part of the experimental program was the study of mean flow characteristics produced by the screen. The measurements included the mean velocity profile and turbulence intensity measurements. The rake with 40 tubes spaced 3/4 in. apart was extensively used for the mean velocity profile measurements. In the final calibrations, a 3/8 in. pitot static tube was measured in the upper half only. Similarly the hot wire probe was also traversed in the upper half. The spanwise velocity profile was measured with the help of horizontal rake mounted on the vertical rake. This was done at three vertical locations. Static pressure measurements were taken using pitot static tube. Flow angle measurements were taken using the cylindrical flow angle probe mentioned earlier.

The second part consisted of taking the pressure distribution data on both the airfoils in uniform flow and nonuniform strong shear flow. Pressure distribution data in shear flow was taken for an angle of attack range of $+ 30^{\circ}$ to $- 20^{\circ}$. For each airfoil this data was taken at seven vertical locations; $y = 0"$, $y = \pm 1"$, $y = \pm 2"$, $y = \pm 4"$. The multitube manometer inclination was kept at 60° with the horizontal during these measurements.

2.3 Data Reduction

The static pressure measurements on the airfoil surface were reduced to the form of aerodynamic coefficients, C_N and C_c, by performing the inte-

gration of pressure coefficients along the X and Y co-ordinates

$$C_N = -\int_0^1 (C_{pu} - C_{pl}) d (x/c) \qquad (2.3)$$

$$C_c = \int C_p \, d(y/c) \qquad (2.4)$$

$$C_L = C_N \cos\alpha - C_c \sin\alpha \qquad (2.5)$$

$$C_D = C_N \sin\alpha + C_c \cos\alpha \qquad (2.6)$$

where α is the angle of attack.

The pitching moment about the leading edge is given by

$$C_{M_{L.E.}} = \int_0^1 \Delta C_p \, (x/c) d(x/c) + \int \Delta C_p (y/c) d(y/c) \qquad (2.7)$$

where nose up pitching moments are positive. Normally these integrations are performed graphically. In the present work these integrations were performed numerically on an IBM 7044/1401 computer, installed at the IIT/Kanpur Computer Centre.

CHAPTER 3

RESULTS AND DISCUSSION

331. Mean flow Characteristics of Non Uniform Strong Shear Flow

a. Mean Velocity Profile.

Two different probes were used to obtain the data on the mean velocity profile of nonuniform strong shear flows. These were a pitot static tube and a pitot rake. Fig. 6 shows the data obtained by the two probes. Data trends are generally satisfactory. The two different probes give more or less the same data. Actually while running the experiment we observed that rake data show a certain amount of asymetry. At times the pitot rake data exhibited asymetry and at other times it did not. This leads us to the conclusion that there is a slight unsteadiness in the mean flow. The data in Fig. 6 show a maximum velocity of 110 ft/sec at y/b = 0.250 and a minimum velocity of 40 ft/sec at the centreline at y/b =0. By comparison in Sharma's[16] work a maximum velocity of 125 ft/sec was obtained at y/b = 0.3 and a minimum velocity of 103.5 ft/sec at the centreline. The velocity profile from the centreline to the peak can be approximated by a parabolic expression such as

$$U = U_c \left(1 + \frac{q}{2} \left(\frac{y}{H} \right)^2 \right) \qquad (3.1)$$

where U_c is the velocity at y/b = 0, q is the shear parameter and H is a transformation length which is equal to 1.7 in. for the 6 in. chord airfoil (see Refs. 3,4). Thus for the present nonuniform shear flow the value of q obtained from the above equation turns out to be .282. In Gupta and Sharma's[17] work the corresponding value was 0.0476. Thus the present shear flow is about an order of magnitude stronger than the earlier flow. On the other hand if we assume the velocity profile to be linear then using the following equation

$$U = U_c \left(1 + \frac{Ky}{c} \right) \qquad (1.1)$$

We get the value of K, the linear shear parameter to be 1.75. In Sharma's[16] work using a linear relationship he obtained a value of K = 0.34.

b. Static Pressure Distribution.

Fig. 7 shows the static pressure distribution. The ratio y/b has been plotted $p/p_{(y/b)=0}$. As is clear from the figure the variation is constant within $\pm$ 4%. The static pressure variation in Gupta and Sharma's[17] case was also small and was nearly constant around the ratio 1.0 within 2%.

c. Streamwise Turbulence Intensity.

Fig. 8 shows the variation of streamwise turbulence intensity U_{rms} plotted against y/b. The root mean square velocity U_{rms} appears to have a maximum value of 40 fps at y/b = 0.167. In this region of high shear the percentage of turbulence is high. It is found to be of the order of 30-50%. In this Sharma's[16] work the maximum value of U_{rms} was 8 fps and the maximum percentage of turbulence was around 10%.

d. Two Dimensionality of the Flow.

The mean flow velocity profile data in the spanwise direction at three vertical locations are shown in Fig. 9. Here the ratio U/U_c has been plotted against y/b. U_c is the velocity of the flow at the central point of the horizontal pitot rake. The three vertical locations for which the velocity profiles are shown are y/b = 0.328,, y/b = 0.0156 and y/b = -0.328. These profiles have been measured 36 in. downstream of the screen. Boundary layers appear to be very thick, of the order of 4 in. or more and are most probably turbulent. The central core or uniform flow region is rather small. In Sharma's[16] work the mean velocity profile in the spanwise direction was measured at only one location, y/b = 0, 36 in. downstream of the screen. The boundary layers on the side walls were about 3 in. thick and were also most probably turbulent. The central 6 in. core of the flow in his case had a uniform velocity within 2%. In the present case the central 2-4 inches of core has a velocity uniform to within $\pm$ 5% .

e. Flow Angle.

Fig. 10 shows the variation of flow angle vs y/b. In the present case the flow angle variation came to be rather large. The flow angle was measured

by means of a cylindrical probe with two pressure holes of 0.02 in. diameter spaced 72° apart. When flow angle is measured with this type of probe it will indicate an apparent flow angle. This probably is partly the reason for high flow angle values. Furthermore, cylindrical probes in high turbulence and unsteady flow are known to give highly erroneous readings. We believe, therefore, that high values of flow inclination shown in Fig. 10 are probably not the true flow inclinations.

5.2 Lift Coefficient Variation With Angle of Attack

Figures 11-18 show the lift coefficient variation plots for symmetric and cambered airfoils. The pressure distribution data were recorded for an angle of attack range of + 30° to - 20°.

a. Symmetric Airfoil.

Fig. 11 presents the C_L vs α plots for the symmetric airfoil in uniform flow and nonuniform strong shear flow for the vertical location y = 0, that is, when the airfoil is mounted at the flow centreline. There are two plots for uniform flow, oneobtained from theory and another from experimental data. The theory plot has been presented for comparison. The figure clearly shows that for shear flow for the vertical location y = 0, the value of C_L is considerably less than the C_L value in uniform flow. For uniform flow the variation of the lift coefficient for the curve obtained from experimental data in the angle of attack range of -10° to + 10° is almost linear. Beyond this, however, the pattern changes. For shear flow the curve varies nearly linearly for the angle of attack range - 10° to + 20°.

Comparing with Sharma's[16] work we see that in his case the C_L values for the symmetric airfoil in nonuniform weak shear flow were more than the C_L values in uniform flow when the C_L values were computed using the midchord dynamic pressure. However, when the stagnation streamline dynamic pressure was used for computing the lift coefficients the C_L values obtained were less than those in uniform flow. In the present case we find that all the C_L

values we have obtained for the symmetric airfoil in nonuniform strong shear flow are less than those in uniform flow.

Effect of Vertical Location

Figures 12, 13 and 14 show C_L vs α plots for the vertical locations $y/b = \pm 0.041, \pm 0.083$ and ± 0.167 for the symmetric airfoil. The effect of vertical location on the maximum lift available is very pronounced. In all three figures the C_L values for a location below the centreline are always higher than the C_L values for a corresponding location above the centreline. Comparing the three figures to one another one sees that the maximum lift available seems to increase as the airfoil is placed further and further away from the flow centreline. In Fig. 12 both the plots appear to be linear for most of the angle of attack range but in Fig. 13 for $y/b = \pm 0.083$ both the curves show a sudden rise near $\alpha = 0^\circ$. In Fig. 14 for the vertical location $y/b = -0.167$ the C_L curve is almost linear before it reaches a plateau but the C_L curve for $y/b = 0.167$ varies oddly. In both Figs. 13 and 14 one sees that near $\alpha = 30^\circ$ the C_L values for both the curves are almost the same.

b. Cambered Airfoil.

Fig. 15 presents the C_L vs α plot for the cambered airfoil in uniform flow and nonuniform strong shear flow for the vertical location $y = o$. The C_L curve obtained from theory has also been presented. The C_L curve obtained from experimental data varies from $\alpha = -20^\circ$ to $\alpha = +12^\circ$ in a more or less linear manner beyond which it falls sharply, reaches a plateau, rises slightly gradually and then again falls. The shear flow curve varies initially from $\alpha = -20^\circ$ to $\alpha = 5^\circ$ in a linear fashion and then rises gradually in a wavy fashion. It is clear from the figure that in nonuniform strong shear flow C_L values fall considerably compared to C_L values in uniform flow.

Effect of Vertical Location

Figures 16, 17, and 18 show the C_L values obtained when the cambered airfoil is placed at the vertical locations $y/b = \pm 0.041, \pm 0.083$ and ± 0.167.

In each of these figures the C_L values for the vertical location below the flow centreline appears to be considerably higher than those for the corresponding vertical location above the flow centreline. for most of the angle of attack range. The curves also tend to vary considerably in shape. In Fig.17 the C_L plot for y/b = - 0.083 assumes a curious ~~hemispherical~~ Semicircular shape in the angle of attack range $\alpha = 7.5^\circ$ to 27.5°. Before this range it follows a more or less linear pattern.

Effect of Camber.

The effect of camber in the cambered airfoil is pretty well pronounced when compared to the symmetric airfoil. C_L values for the cambered airfoil both in uniform flow and in shear flow are considerably higher than the corresponding C_L values for the symmetric airfoil. The difference is particularly marked in shear flow.

3.3 Pitching Moment Coefficient Variation With Angle of Attack

Figures 19-26 show the variation of the pitching moment coefficient at the leading edge with the angle of attack for symmetric and cambered airfoils. The pressure distribution data were recorded for an angle of attack range of $+ 30^\circ$ to $- 20^\circ$.

a. Symmetric Airfoil.

Fig. 19 shows the $C_{M_{L.E.}}$ (C_M at leading edge) vs α plot for the symmetric airfoil in uniform flow and in nonuniform strong shear flow at the vertical location y = 0. Except for a small angle of attack range close to $\alpha = 0^\circ$ where the two curves almost coincide the curves diverge quite a bit. For values of α less than 0° the $C_{M_{L.E.}}$ values for uniform flow are higher than $C_{M_{L.E.}}$ values for shear flow, whereas for values of $\alpha > 0^\circ$ the $C_{M_{L.E.}}$ values for shear flow are higher than $C_{M_{L.E.}}$ values for uniform flow. The $C_{M_{L.E.}}$ plot for shear flow is almost linear throughout.

Effect of Vertical Location

1 Figs. 20,21 and 22 show the symmetric airfoil in shear flow for the vertical locations $y/b = \pm 0.041$, ± 0.083 and ± 0.167. For the vertical locations $y/b = \pm 0.041$ the two curves almost coincide with each other. The $C_{M_{L.E.}}$ values for $y/b = +0.041$ are only slightly greater than those for $y/b = -0.041$. The curves slope down from left to right. For $y/b = \pm 0.083$ the curves follow a similar trend. However the $C_{M_{L.E.}}$ values for $y/b = +0.083$ are distinctly greater than those for $y/b = -0.083$ although the differences are small. Both the curves are almost linear and slope down from left to right.

A similar trend is observed in Fig. 22 where $C_{M_{L.E.}}$ vs α for the vertical locations $y/b = \pm 0.167$ are plotted. Near $\alpha = +5$ the two curves appear to converge and then diverge again. Comparing the Figs. 20, 21 and 22 it appears that $C_{M_{L.E.}}$ values for vertical locations above and below the centre-line are more or less close in magnitude for all the three figures. Comparing Fig. 19 with Figs. 20, 21 and 22 we see that compared to uniform flow $C_{M_{L.E.}}$ values in shear flow differ markedly. For $\alpha < 0^\circ$ the $C_{M_{L.E.}}$ values for uniform flow are greater than those in shear flow for all the vertical stations and for $\alpha > 0^\circ$ the $C_{M_{L.E.}}$ values for uniform flow are less than those in shear flow for all the vertical stations. In other words the $C_{M_{L.E.}}$ vs α curve for uniform flow is a much more steep curve sloping down from left to right, compare to the shear flow curves. This has important consequences on the stability of the wing. This implies that a wing with a symmetrical Joukowsky airfoil is likely to be less stable in nonuniform strong shear flow than in uniform flow.

b. Cambered Airfoil.

Fig. 23 shows the $C_{M_{L.E.}}$ vs α plot for the cambered airfoil in uniform flow and in shear flow for the vertical location $y = 0$. The uniform flow curve differs markedly from the uniform flow curve for the symmetric airfoil. The uniform flow curve for the cambered airfoil lies entirely below the shear

flow curve. The shear flow curve is approximately linear and slopes down gently from left to right. Both the curves lie below the abscissa, that is, the $C_{M_{L.E.}}$ values for both uniform and shear flow are negative for the entire angle of attack range.

Effect of Vertical Location

Figures 24, 25 and 26 show the $C_{M_{L.E.}}$ vs α plots for the cambered airfoil in nonuniform strong shear flow for the vertical locations $y/b = \pm 0.041$, ± 0.083 and ± 0.167. In all the three plots the curves are pretty close to each other for most of the angle of attack range. In Figures 24 and 25 the curves almost coincide from $\alpha = -20^{\circ}$ to $\alpha = +5^{\circ}$, but diverge after that. In all three figures the curves slope down gently from left to right and all the curves stay below the abscissa indicating that the $C_{M_{L.E.}}$ values in all the plots are negative. The closeness of the curves indicates that there is very little difference in $C_{M_{L.E.}}$ values for two corresponding vertical locations above and below the centreline. However in all the three figures the curve for the positive vertical location ($y/b = 0.041, 0.083, 0.167$) stays slightly above the curve for the negative vertical location which is in keeping with the trend observed so far.

Comparing to the uniform flow curve one sees that all the curves in simi shear flow lie above the uniform flow curve. This indicates that $C_{M_{L.E.}}$ values obtained in shear flow are considerably higher than $C_{M_{L.E.}}$ values in uniform flow.

Effect of Camber

The most noticeable effect due to camber is that the values of $C_{M_{L.E.}}$ are lowered considerably for the entire angle of attack range. This is true for both shear flow and uniform flow. Comparing corresponding curves in shear flow and uniform flow for both the airfoils one sees that in case of the cambered airfoil the maximum $C_{M_{L.E.}}$ obtained is considerably less than the maximum $C_{M_{L.E.}}$ values obtained for the symmetric airfoil for the same vertical

locations in shear flow and also in uniform flow. The slopes of the $C_{M_{L.E.}}$ ~~covers~~ Curves for the cambered airfoil, however, appear to be more or less the same as those for the symmetric airfoil.

3.4 Variation of Pressure Drag Coefficient with Angle of Attack

Figs. 27 and 28 show the variation of the pressure drag coefficient with the angle of attack for the symmetric and cambered airfoils respectively. In each figure only two plots have been shown, one for uniform flow and one for shear flow when the airfoil is located at the flow centreline, that is $y = 0$. In both figures the uniform flow curve shows a distinct bucket like shape. When shear is introduced in both cases the curve tends to flatten as the curves for shear flow show. The shear flow curve is both cases stays entirely above the abscissa but the uniform flow curve strays below the abscissa for both airfoils. Appearance of a negative pressure drag coefficient is likely to be due to the assumption of ambient pressure at the trailing edge and discrete nature of data causing errors in numerical integration.

3.5 Typical Pressure Distributions

A large number of pressure distributions were recorded over the two airfoils for different geometrical angles of attack ranging from $+ 30^{\circ}$ to -20° and seven vertical locations. Some typical pressure distributions plots for symmetrical and cambered airfoils measured in uniform flow and shear flow for various vertical locations are presented in Figs. 29 to 34. The dotted lines show that the data for these regions are not available and hence a dotted line is drawn from the las available data point to the trailing edge. Pressure distributions for each airfoil have been presented for five vertical locations; $y/b = 0, \pm 0.041$ and ± 0.167. The pressure coefficient C_p is based on the midchord dynamic pressure at that particular vertical location. It has been suggested that the dynamic pressure of the stagnation streamline be used for computing the aerodynamic coefficients. Since the exact location of the

stagnation streamline was difficult to determine, Ludwig and Erickson[6] used the difference between the free stream static pressure and the pressure on the leading edge position of the airfoil, as the stagnation streamline dynamic pressure. In the present work we took the average value of the static pressure over the entire range of experimentation ($\alpha = +30^\circ$ to $\alpha = -20^\circ$), and subtracted the total pressure at the airfoil midchord location to get the dynamic pressure. The total pressure value was obtained at different vertical locations using the Pitot rake data.

a. Symmetric Airfoil.

In Fig. 29 $-C_p$ vs x/c for the symmetric airfoil in uniform flow and in nonuniform strong shear flow with the airfoil at y = 0, that is at the centre-line, has been plotted. The plots have been presented for the geometrical angles of attack $\alpha = 0^\circ$, 4°, 12° and 20°. The value of q obtained earlier has been found to be 0.282.

Data in Fig. 29 show that as the geometrical angle of attack increases the minimum pressure point moves forward for uniform flow. The $-C_p$ values for uniform flow appear to be greater compared to the $-C_p$ values of shear flow for $\alpha = 0^\circ$ and $\alpha = 4^\circ$. However for $\alpha = 12^\circ$ and $\alpha = 20^\circ$ only the $-C_p$ values for the suction on the upper surface appear to be greater than the $-C_p$ values for shear flow. $-C_p$ plots for both the surfaces of the airfoil tend to come closer to each other in shear flow as one moves gradually from $\alpha = 0^\circ$ to $\alpha = 12^\circ$. But for $\alpha = -20^\circ$ they again diverge. The $-C_p$ plot for the upper surface in uniform flow tends to fall gradually across the surface of the airfoil for $\alpha = 0^\circ$, 4° and 12°. For $\alpha = 20^\circ$ the plot falls sharply from the second point to the third point and then rises slightly and that too very gradually across the airfoil surface indicating that the flow has stalled. The $-C_p$ plots for the lower surface for $\alpha = 0^\circ$ and 4° appear above the abscissa while for $\alpha = 12^\circ$ and 20° appear below the abscissa.

Figs. 30 and 31 show the pressure distribution on the symmetric airfoil in nonuniform strong shear flow. In Fig. 30 $-C_p$ has been plotted against x/c for the vertical stations $y/b = \pm 0.041$ for the three geometrical angles of attack $\alpha = 4^\circ$, 10° and 20°. The three plots show a great deal of difference. At $\alpha = 4^\circ$ the peak of the $-C_p$ curve for $y/b = +0.041$ appears to be much higher compared to the peak of the $-C_p$ curve for $y/b = -0.041$. At $\alpha = 10^\circ$ and 20° the peaks of the $-C_p$ curves for $y/b = -0.041$ are higher than the peaks of the $-C_p$ curves for $y/b = 0.041$. At $\alpha = 4^\circ$ and 20° the variation in $-C_p$ appears to be uniform for both $y/b = -0.041$ and $y/b = +0.041$. The curves fall graduall initially and then as the trailing edge approaches they rise gradually again. At $\alpha = 10^\circ$ however the pattern of variation tends to be erratic, some of the curves fall suddenly, rising immediately again, falling again, reaching a plateau, and as the trailing edge approaches again rise gradually.

Fig. 31 shows the symmetric airfoil in shear flow at the vertical locations $y/b = \pm 0.167$. Plots have been presented for the angles $\alpha = 4^\circ$, 10° and 20°. The peak value of the $-C_p$ curve for the upper surface of the airfoil for $y/b = -0.167$ is higher for all three values of α than the peak value of $-C_p$ for the upper surface for $y/b = 0.167$. The trend of the plots here is somewhat different than the plots for $y/b = \pm 0.041$. For the vertical locations $y/b = \pm 0.041$ most of the data points tended to be concentrated below the abscissa whereas for the vertical locations $y/b = \pm 0.167$ the points are more evenly spread.

Effect of Stream Shear

Ludwig and Erickson[6](1971) have concluded that the change in lift is mainly due to upper surface pressure distribution. In the present case pressu distributions over the symmetric airfoil as shown in Figs. 29-31, indicate that nonuniform stream shear brings about a change in both the upper and lower surface pressure distributions. This is true for both the vertical stations $y/b = \pm 0.041$ and ± 0.167. In Sharma's work it was noticed that nonuniform stream shear brings about a change in the suction pressure on the upper surfac Shar

Sharma[16] also reported that a study of the lower surface pressure distribution didnot show any significant change due to stream shear. However in the present case a close scrutiny reveals that although lower surface pressure does not change appreciably for some cases, it does change considerably for others (Fig. 29 and 30). This is particularly true when the airfoil is mounted in shear flow at the centre of the tunnel test section. For the y = 0 location one sees (Fig. 29) that the high nonuniform stream shear does change the pressure distribution for both the surfaces considerably.

Effect of Vertical Location

Comparing Fig. 29 with the Figs. 30 and 31 we see that vertical location has a marked effect on the pressure distribution pattern. Comparing the pressure distribution plots of $y/b = \pm 0.041$ and ± 0.167 in shear flow with the pressure distribution plots of the vertical location y = 0. we see as we move away from the flow centreline the suction on the upper surface increases considerably. The pressure distribution on the lower surface also changes considerably.

b. Cambered Airfoil.

Figs. 32-34 show the pressure distribution plots for the cambered airfoil for q = .282. Fig. 32 shows the plots for uniform flow and shear flow for the vertical location y = o. Plots have been presented for $\alpha = 0^\circ, 4^\circ, 10^\circ$ and 20°. In uniform flow there is a tendency for the pressure peaks to move forward for both the upper surface and lower surface as the angle of the attack increases. At $\alpha = 0^\circ, 4^\circ$ and 10° the upper surface curves for uniform flow rise and fall gradually, but for $\alpha = 20^\circ$ the upper surface curve behaves rather differently. It falls sharply almost from the beginning and then levels off indicating stalling. In shear flow the curves for both the upper and the lower surfaces appear to be below. the absicissa for most of the surface. The $-C_p$ plot for the upper surface in shear flow at $\alpha = 20^\circ$ differs markedly from the rest. At x/c = .4 it falls sharply and then levels off at a nearly

constant value indicating stalling.

Figs. 33 and 34 show the $-C_p$ vs x/c plots in nonuniform strong shear flow for the cambered airfoil for the vertical locations $y/b = \pm 0.041$ and ± 0.167. Plots for the angles $\alpha = 4^\circ$, 10° and 20° have been presented. The figures for the three angles differ markedly from each other. This is true for both $y/b = \pm 0.041$ and $y/b = \pm 0.167$. For $y/b = \pm 0.041$ suction over the upper surface seems to increase considerably at $\alpha = 10^\circ$ compared to $\alpha = 4^\circ$ but again decreases at $\alpha = 20^\circ$. This seems to be true for $y/b = \pm 0.167$ also.

Effect of Stream Shear

The pressure distribution of the cambered airfoil shows a fall in the suction pressure over the upper surface in nonuniform shear flow compared to the pressure distribution over the upper surface in uniform flow. This is true for both $y/b = \pm 0.041$ and $y/b = \pm 0.167$ as well as $y/b = 0$.

Effect of Vertical Location

Comparing Figs. 33 and 34 with Fig. 32 we see that the pattern of pressure distribution changes considerably with change in vertical location. Peaks become more clearly distinguishable when one moves from $y = 0$ to $y/b = \pm 0.041$. As one moves further to $y/b = \pm 0.167$ the peaks become more sharp with sharp rises and falls. The suction on the upper surface also increases as one moves further away from the centre.

Effect of Camber

Comparing Figs. 29 and 32 we see that camber changes the pressure distribution pattern considerably, both for uniform and shear flow for the vertical location $y = 0$. Camber tends to move the suction peak on the upper surface further down the airfoil surface. It also changes the pressure distribution on the lower surface considerably.

Comparing Figs. 30 and 33, and 31 and 34 one sees that for shear flow too, camber changes the pressure distribution considerably. Suction on the upper surface of the cambered airfoil particularly appears to be more when compared to the suction on the upper surface of symmetrical airfoil.

CHAPTER 4

CONCLUSIONS AND SUGGESTIONS FOR FURTHER WORK

In view of the experiments carried out in the Reynolds no. range of $1.27 \times 10^5 - 3.49 \times 10^5$ the following conclusions can be drawn.

(i) A screen was made which gave nonuniform strong shear flow. But certain problems were encountered, mainly asymetry of the mean flow. The asymetry was present at times and absent at other times. This leads one to the conclusion that there was some unsteadiness. The asymetry was not due to the rods as the rods were positioned symmetrically very accurately.

(ii) A model incidencesystem was designed and fabricated to provide a digital readout with an accuracy of 1/10th of a degree and it worked reasonably well.

(iii) The flow angle values obtained were unreasonably large. It is not certain whether they were really large. As mentioned earlier cylindrical probes in highly turbulent and unsteady flows are known to give highly erroneous readings. So it remains to be determined whether the flow angles are really large.

(iv) Comparedto uniform flow general lift characteristics go down when strong shear is introduced. The maximum C_L values obtained are lower with higher shear. When the airfoil is mounted ata location above or below the flow centre line, however, the maximum lift available is more compared to the maximum lift available when the airfoil is mounted at the flow centreline. As reported in earlier works, for vertical locations below the centreline the maximum lift obtained is more than the maximum lift obtained for a corresponding location above the flow centreline. It is also noticed that as the airfoil moves further away from the centreline the maximum lift available increases. In Gupta and Sharma's[17] work the maximum C_L values were obtained mostly in the angle of attack range $\alpha = 10^\circ$ to 16° where as in the present work the maximum C_L value obtained is usually around 30°.

(v) Like the symmetric airfoil the general lift characteristics of the cambered airfoil compared to uniform flow go down when strong shear is intro-

duced. Here too the maximum C_L values obtained are lower with higher shear. As reported in earlier works when the airfoil is mounted below the centreline the maximum lift obtained is greater than the maximum lift for a corresponding location above the centreline but the difference is greater than in the case of the symmetric airfoil. The maximum values of C_L are reached usually between 20° and 30°.

(vi) For the symmetric airfoil in uniform flow the $C_{M_{L.E.}}$ vs α curve slopes down from left to right indicating a configuration which is stable from the point of view of stability. However, when strong shear is introduced the slope decreases and the $C_{M_{L.E.}}$ vs α curve tends to have a less slope, which means that in nonuniform strong shear flow the wing is going to be less stable compare to uniform flow, though of course, it will still be stable and not unstable. When one moves away from the flow centreline the curves still slope down from left to right indicating that the wing is stable.

The curve for a vertical location above the flow centreline tends to stay above the curve for a corresponding vertical location below the flow centreline. Also as one moves further away from the flow centreline the curve for a location above the centreline tends to pitch away from the abscissa indicating a more stable configuration. The curve for a location below the centreline tends to pitch closer to the abscissa as one moves away from the centreline indicating a less stable configuration.

(vii) For the cambered airfoil the $C_{M_{L.E.}}$ vs α curve also slopes down from left to right but it does so in an odd fashion. When strong shear is introduced and the airfoil is mounted at the flow centreline the entire $C_{M_{L.E.}}$ vs α curve rises vertically well above the uniform flow curve. It still slopes down from left to right indicating a stable configuration but the slope is not very high. When one moves away from the flow centreline the $C_{M_{L.E.}}$ vs α curv for vertical locations both above and below the centreline slope down from left to right (though sometimes in an odd fashion) indicating stable configura-

tions. The plots for locations both above and below the centreline stay close to each other indicating there is little difference in stability for two vertical locations located above and below the centreline but at an equal distance. The slopes of the curves also appear to increase slightly as the airfoil is moved away from the centreline.

Suggestions For Further Work

1. Mean flow angle properties should be studied carefully. A study should be carried out to find out how flow develops into shear flow and explain the reason for the asymetry and large flow inclinations which have been observed.

2. Oil film flow visualisation studies should be made to visualize the separation of the boundary layer and to study the stalling characteristics.

3. A theoretical and numerical investigation along the lines of Ludwig and Erickson[6] may be carried out to check the experimental results and obtain better understanding of the aerodynamic characteristics of airfoils in nonuniform shear flow.

REFERENCES

1. Tsien, H.S., 'Symmetrical Joukowsky Airfoils in Shear Flow', Quart. App. Maths., Vol 1, pp 130-148, 1943.

2. Sowyrda, A., 'Theory of Cambered Joukowsky Airfoils in Shear Flow', Cornell Aeronautical Laboratory Report No. AI-1190-A-2, September 1958.

3. Jones, E.E., ' The Forces on a Thin Airfoil in Slightly Parabolic Shear Flow'. Z.A.M.M., Vol 37, No. 9-10 pp 362-370, 1957.

4. Vidal, R.J., Hilton, J.H., and Curtis, J.T., 'The Two Dimensional Effects of Slipstream Shear on Airfoil Characteristics'. Cornell Aeronautical Laboratory Report No. AI-1190-A-5, September 1960.

5. Vidal, R.J., 'The Influence of Two Dimensional Stream Shear on Airfoil Maximum Lift'. Journal of Aerospace Sciences, Vol. 29, No.8, pp 889-904, 1962.

6. Ludwig, G.R., and Erickson, J.C. Jr., 'Airfoils in Two Dimensional Nonuniformly Sheared Slipstream'. Journal of Aircraft, Vol. 8., No.11, pp 874-880, November 1971.

7. Taylor, G.I. and Batchlor, G.K., 'The Influence of Wire Gauze on Small Disturbances in Uniform Stream'. Quart. Jour. Mech. and App. Maths., Vol 11, Pt.- 1, pp 1-29, 1949.

8. Owen, P.R., and Zienkiwicz, H.K., 'The Production of Uniform Shear Flow in a Wind Tunnel'. Jour. Fluid. Mech., Vol. 2, Pt. 6, pp 521-531, August 1957.

9. Elders, J.W., 'Steady Flow Through Nonuniform Gauzes of Arbitrary Shapes'. Jour. Fluid. Mech. Vol. 5, pp 355-68.

10. McCarthy, J.H., 'Steady Flow Past Nonuniform Wire Grids'. Jour. Fluid Mech., Vol. 19, pp 491-512, 1964.

11. Kotansky, D.R., 'The Use of Honey Comb for Shear Flow Generation'. A.I. A.A. Journal, Vol. 4, No. 8, pp 1490-91, 1966.

12. Livesay, J.L. and Laws, E.M., 'Simulation of Velocity Profiles by Shaped Gauze Screens', A.I.A.A. Journal, Vol. 11, No. 2, p 184, Feb 1973.

13. Pankhurst, R.C. and Holders, D.W., 'Wind Tunnel Techniques'. Sir Isaac Pitman & Co. , London.

14. Tani, A., 'Low Speed Flow Involving Bubble Separation'. Progress in Aeronautical Sciences, Vol. 5, No. =2, Pergamon Press, 1964.

15. Houghton, E.L. and Brock, A.E., 'Aerodynamics for Engineering Students'. Edward Arnold Ltd., London 1966.

16. Sharma, S.C., 'Pressure Measurements on Joukowsky Airfoils in Nonuniformaly Sheared Flows', M. Tech. Thesis, Dept. of Aeronautical Engineering, I.I.T., Kanpur, India, 1973.

17. Gupta, A.K. and Sharma, S.C., 'Cambered Joukowsky Airfoil in a Nonuniform Weak Shear Flow', Journal of Aircraft, Vol. 11, No.10, pp 653-656, October 1974.

18. CAL/USAAVLABS Symposium Proceedings, 'Aerodynamic Problems associated with V/STOL Aircraft', Vol. 2, Published by CALSPAN Corporation, Buffalo, New Yourk 14221, 1966.

19. Brady, W.G., Ludwig, G.R., 'Theoretical and Experimental Investigation of the Aerodynamic Properties of Airfoils near Stall in a Two Dimensional Nonuniformly Sheared Flow', USAAVLABS Technical Report 66-35, Published by U.S. Army Aviation Material Laboratories, Fort Eustis, Virginia, 1966.

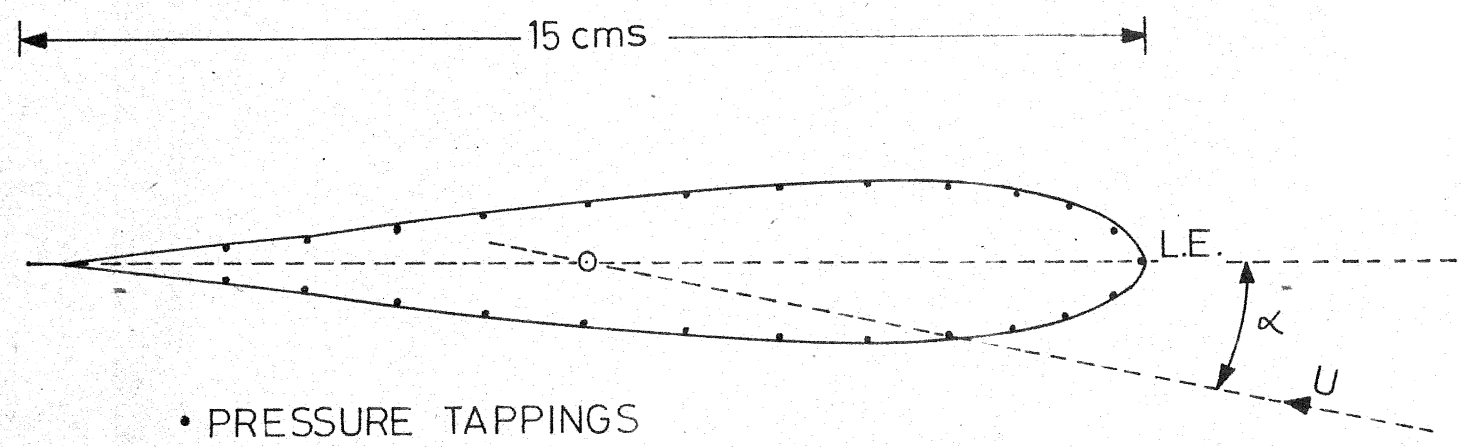

CHORD = 15 cms

THICKNESS = 15%

AIRFOIL CO-ORDINATES

X (CMS)	Y (CMS)
0	O L E
·114	0·298
·452	0·575
1·005	0·808
1·755	0·983
2·679	1·093
3·750	1·125
4·935	1·092
6 198	1·001
7·500	0·866
8·802	0·705
10·065	0·535
11·250	0·375
12·321	0·237
13·245	0 130
14·295	0·058
14·548	0·018
14·886	000 2
15·000	OTE
L E RADIUS ·25 CM	

FIG. 1 – SYMMETRICAL JOUKOWSKY AIRFOIL.

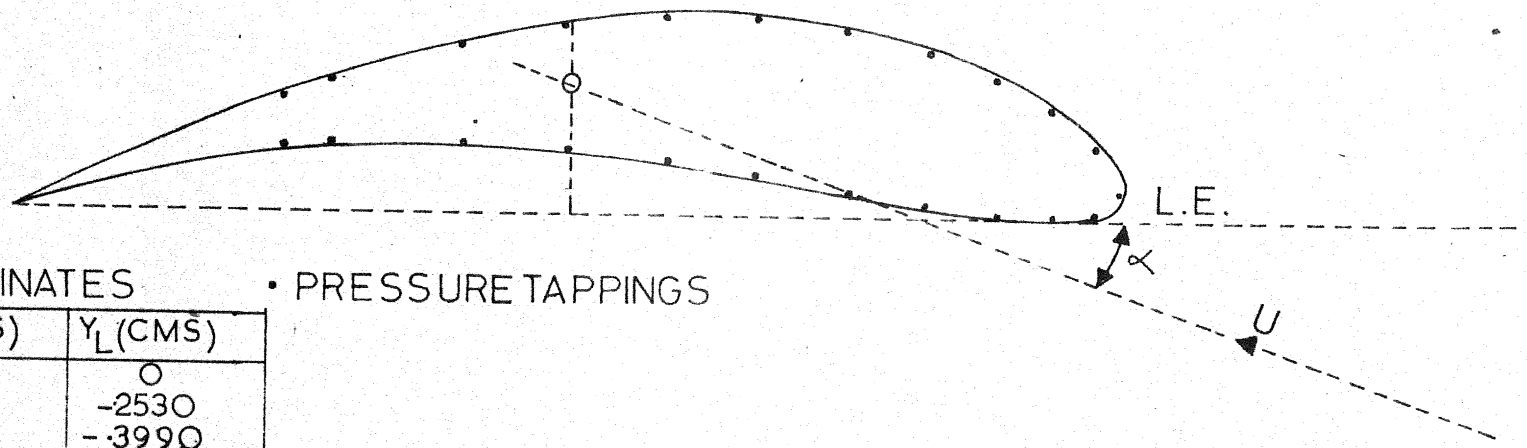

AIRFOIL CO ORDINATES • PRESSURE TAPPINGS

X (CMS)	Y_U (CMS)	Y_L (CMS)
O	O LE	O
0·114	0·3440	-2530
0·452	0·1500	-·3990
1·005	1·1830	-·4330
1 755	1 6030	-·3630
2 679	1·9730	-·2100
3 750	2·2500	·0·000
4·935	2·4170	·2320
6·198	2·4560	·4540
7·500	2·3660	·6340
8·802	2·1600	·1000
10·065	1·8600	·7890
11·250	1·500	·7500
12·321	1·1170	·6430
13·245	0.750	·4900
14·295	0·430	·3170
14·548	0·1930	·1580
14·886	0·0480	·0430
15·000	O TE	O
L E (RADIUS)	·22 CM	

CHORD = 15 CMS
THICKNESS = 15%
CAMBER = 10%

FIG. 2 - CAMBERED JOUKOWSKY AIRFOIL.

1 - BASE PLATE
2 - YOKE
3 - CENTRAL HOLLOW SHAFT
4 - LARGE WORM WHEEL
5 - LARGE WORM SHAFT (NOT SHOWN HERE, SHOWN IN FIG. 4)
6 - SMALL WORM SHAFT
7 - BEVEL GEARS
8 - 5 - DIGIT MECHANICAL REVERSIBLE COUNTER
9 - HANDLE
10 - 360° PROTACTOR (NOT SHOWN HERE, SHOWN IN FIG. 4)
11 - PROTACTOR POINTER (NOT SHOWN HERE SHOWN IN FIG. 4)
12 - MOUNTING HOLDER (NOT SHOWN HERE, SHOWN IN FIG. 4)

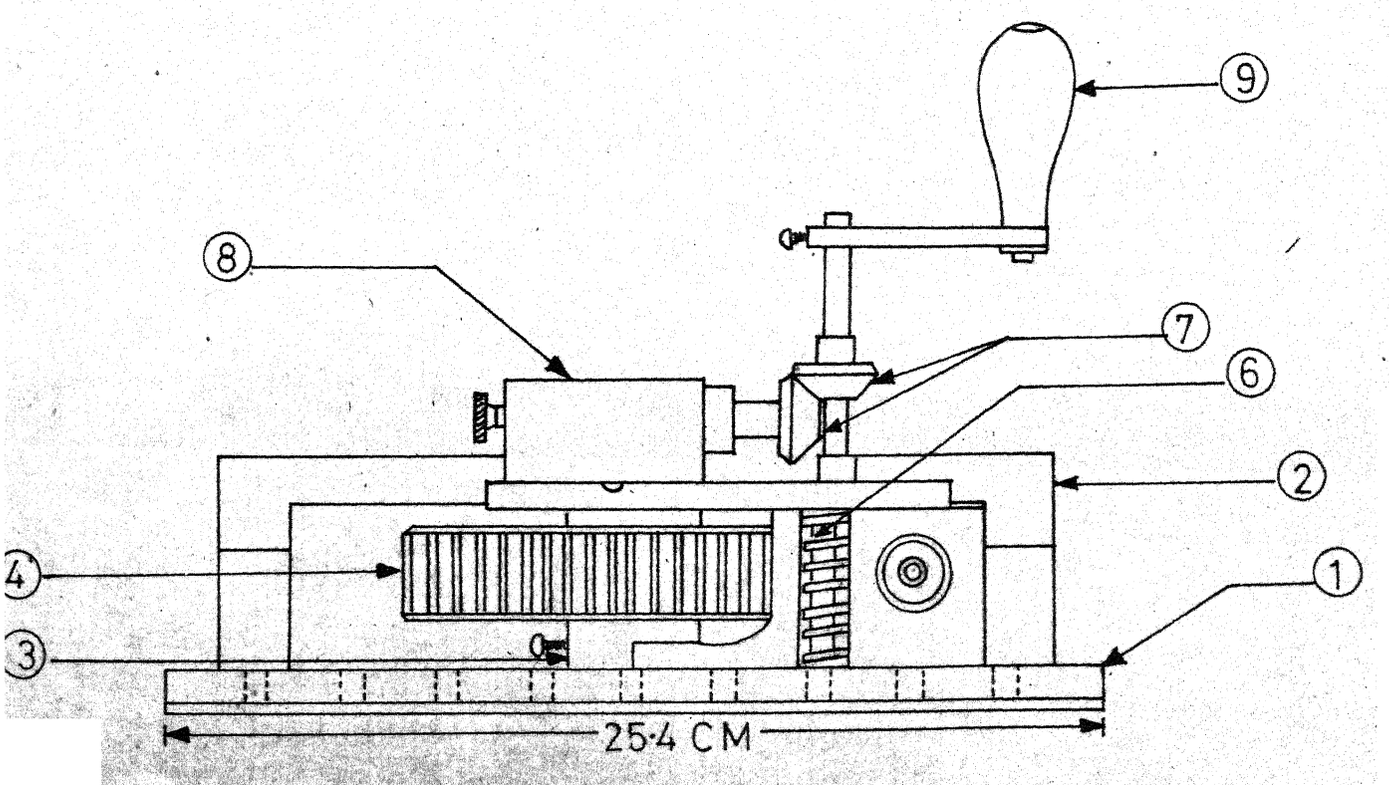

FIG. 3 - SIDE VIEW OF 2-D MODEL INCIDENCE SYSTEM.

1- BASE PLATE
2- YOKE
3- CENTRAL HOLLOW SHAFT
4- LARGE WORM WHEEL
5- LARGE WORM SHAFT
6- SMALL WORM SHAFT (NOT SHOWN HERE SHOWN IN FIG.3)
7- BEVEL GEARS
8- 5 DIGIT MECHANICAL REVERSIBLE COUNTER
9- HANDLE
10- 360° PROTACTOR
11- PROTACTOR POINTER
12- MOUNTING HOLDER

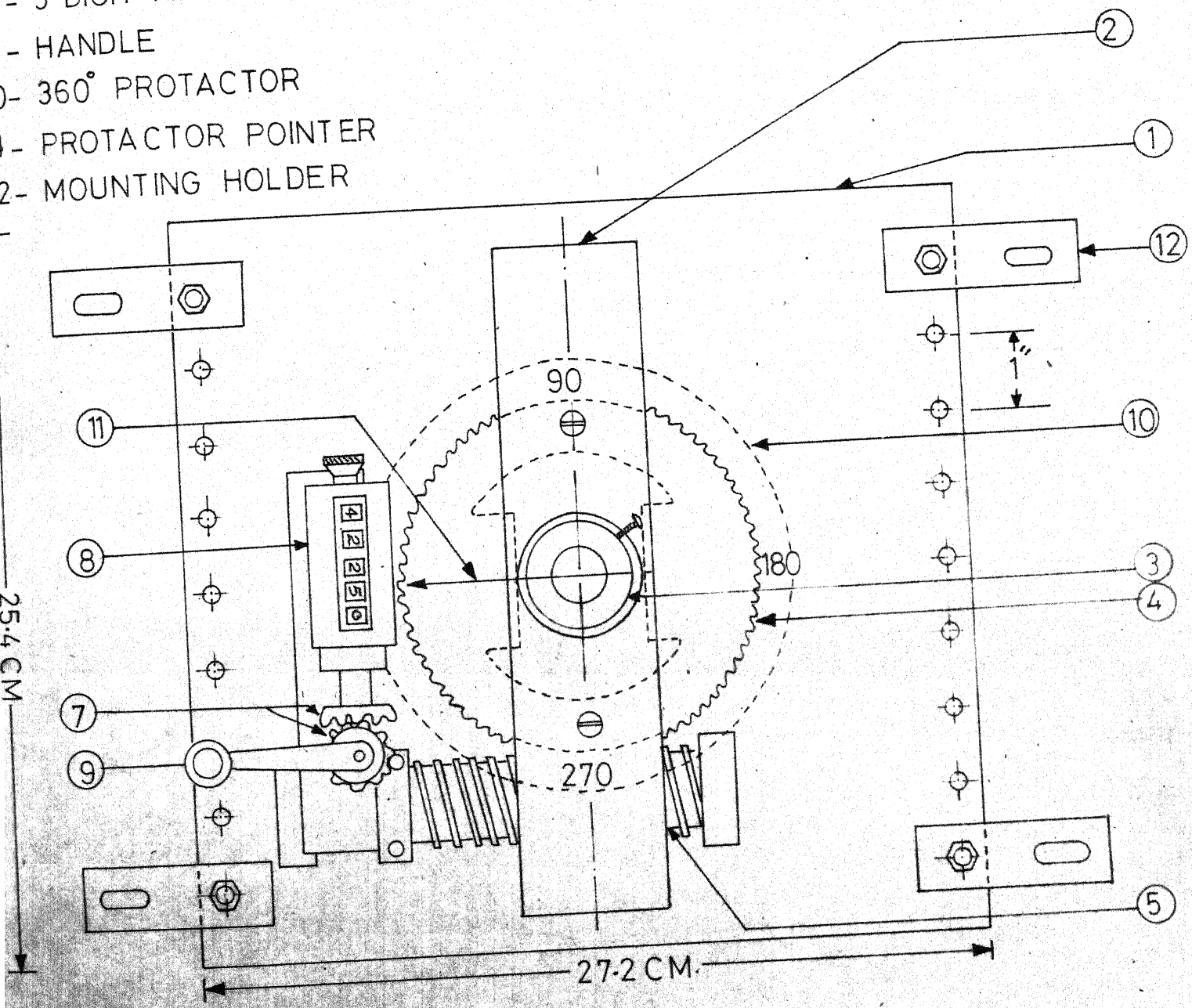

FIG. 4- TOP VIEW OF 2-D MODEL INCIDENCE SYSTEM.

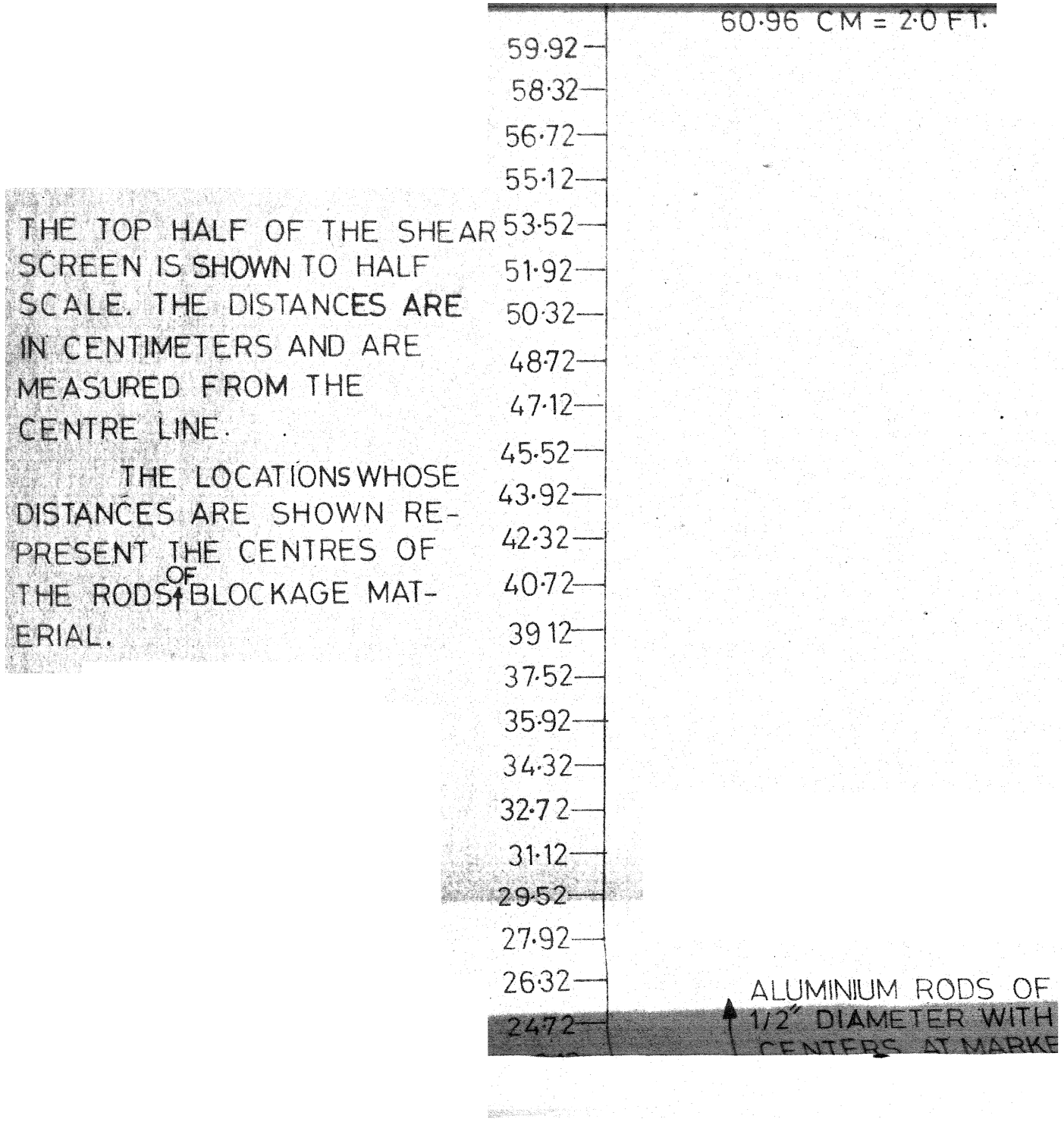

THE TOP HALF OF THE SHEAR SCREEN IS SHOWN TO HALF SCALE. THE DISTANCES ARE IN CENTIMETERS AND ARE MEASURED FROM THE CENTRE LINE.

THE LOCATIONS WHOSE DISTANCES ARE SHOWN REPRESENT THE CENTRES OF THE RODS OF BLOCKAGE MATERIAL.

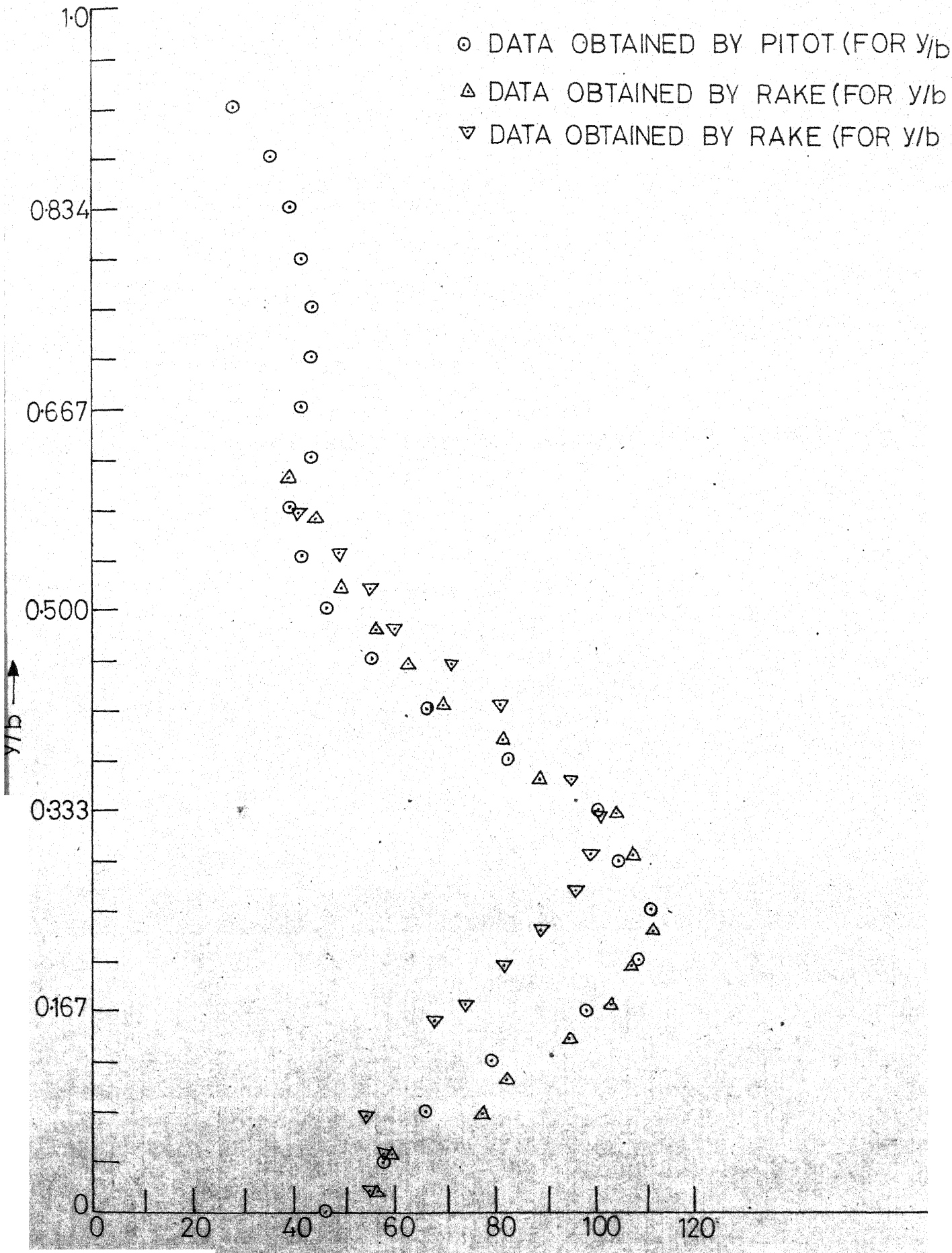
⊙ DATA OBTAINED BY PITOT (FOR y/b >0)
△ DATA OBTAINED BY RAKE (FOR y/b >0)
▽ DATA OBTAINED BY RAKE (FOR y/b <0)
1·0
0·834
0·667
0·500
0·333
0·167
0
y/b
0
20
40
60
80
100
120
U (FT./SEC.)

FIG. 6 - y/b VS U

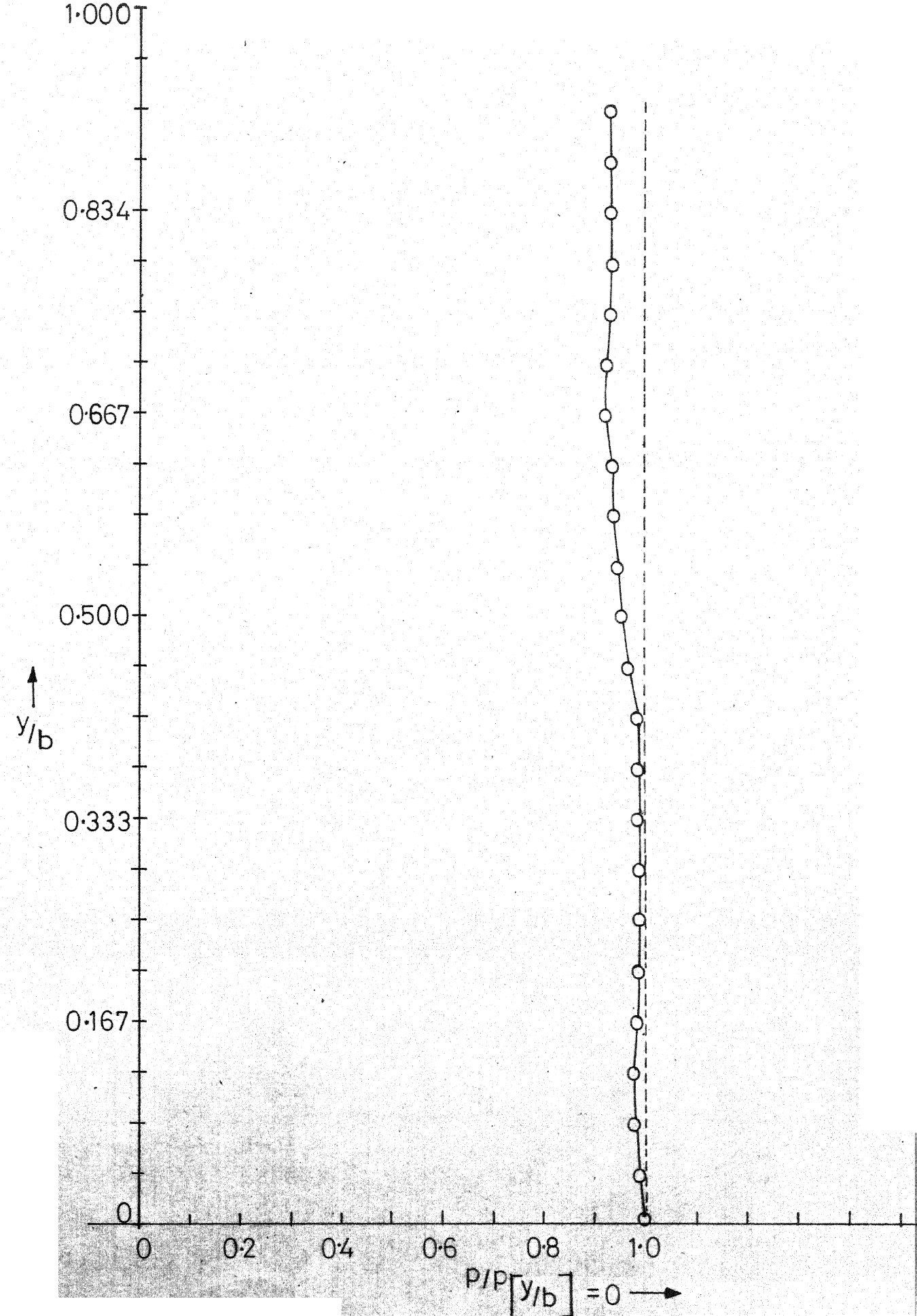

FIG. 7 - y/b VS $p/p_{[y/b]=0}$

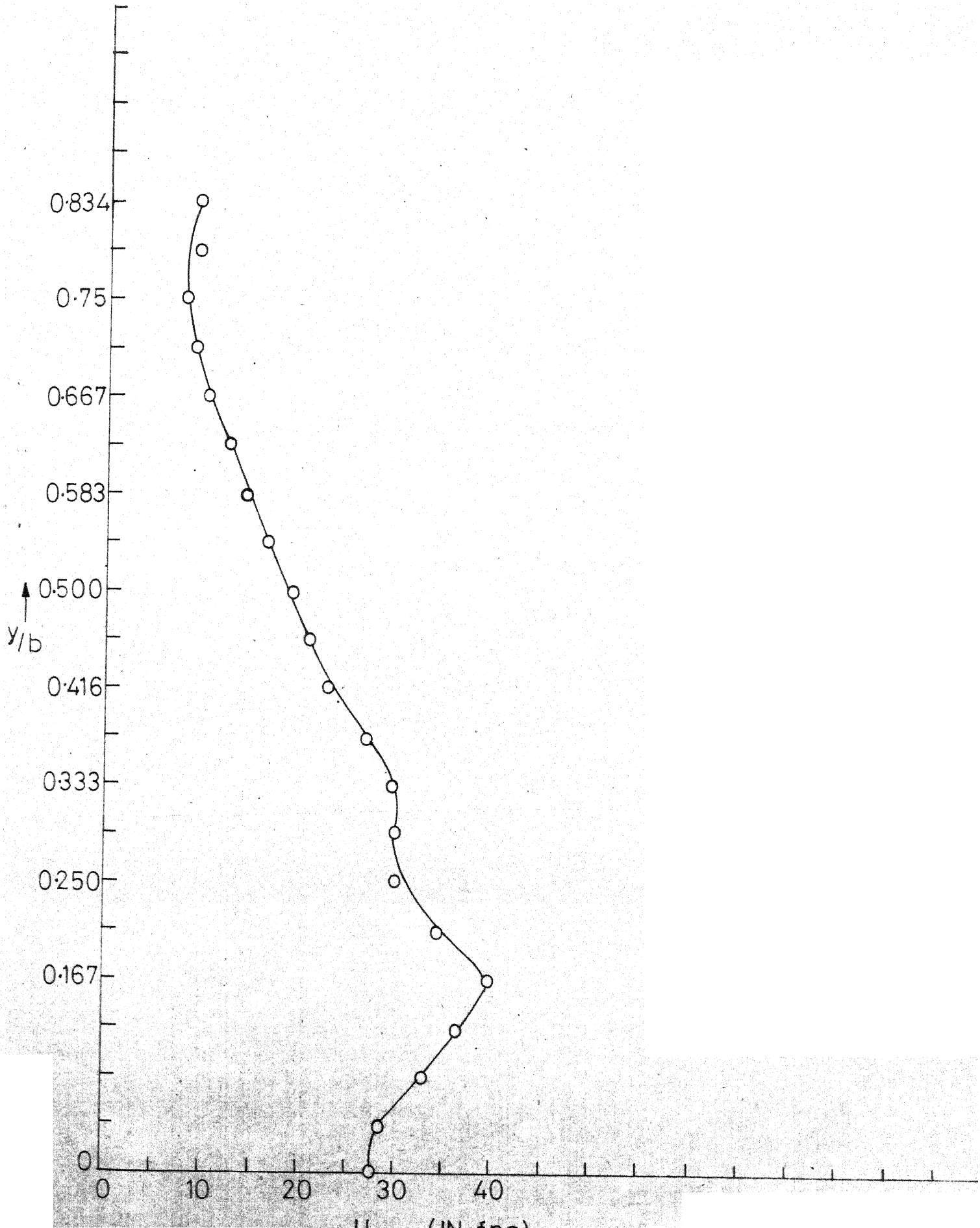

FIG. 8 - y/b VS U_{rms}

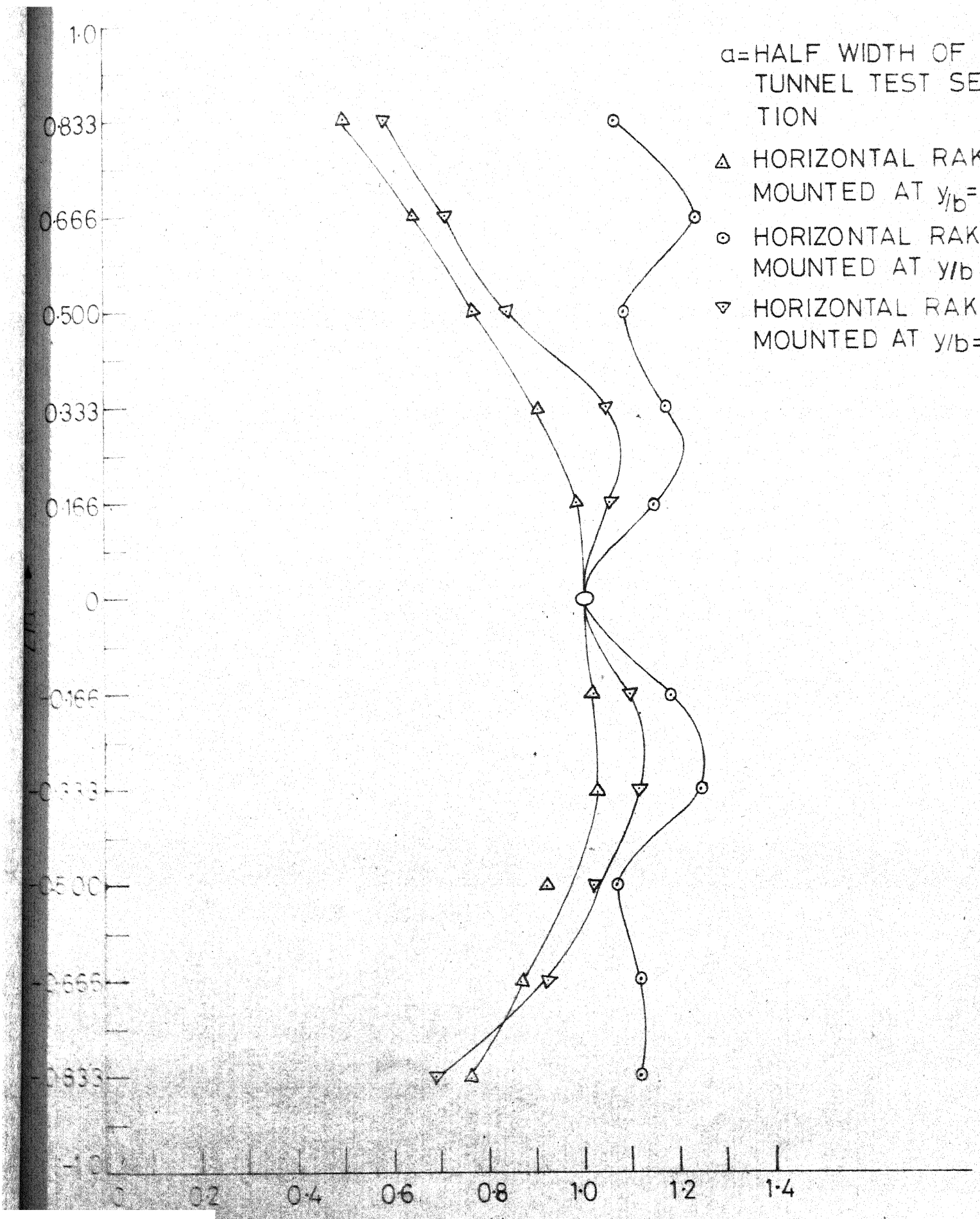

FIG. 9 - Z/a VS U/Uc

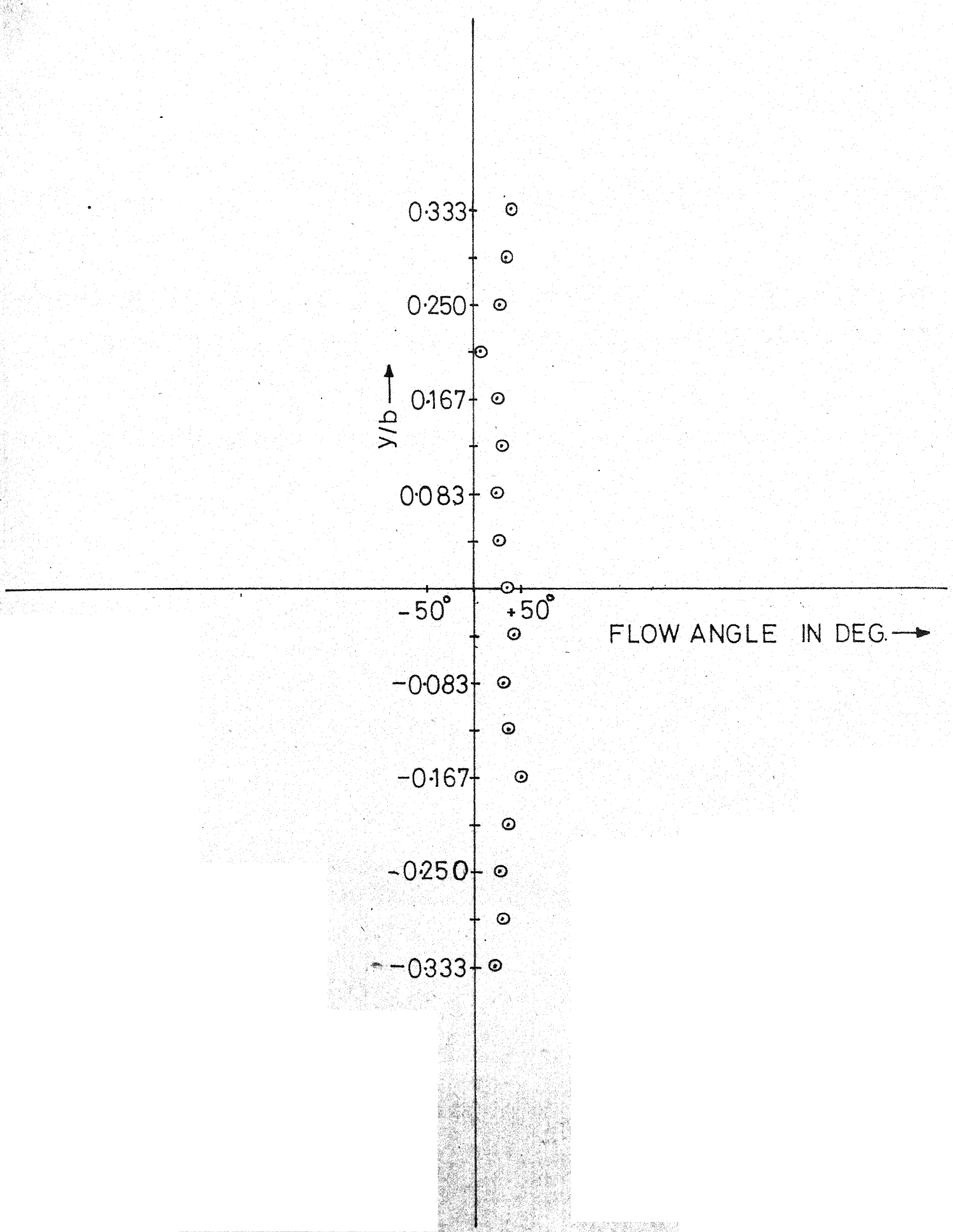

FIG. 10 - y/b VS FLOW ANGLE

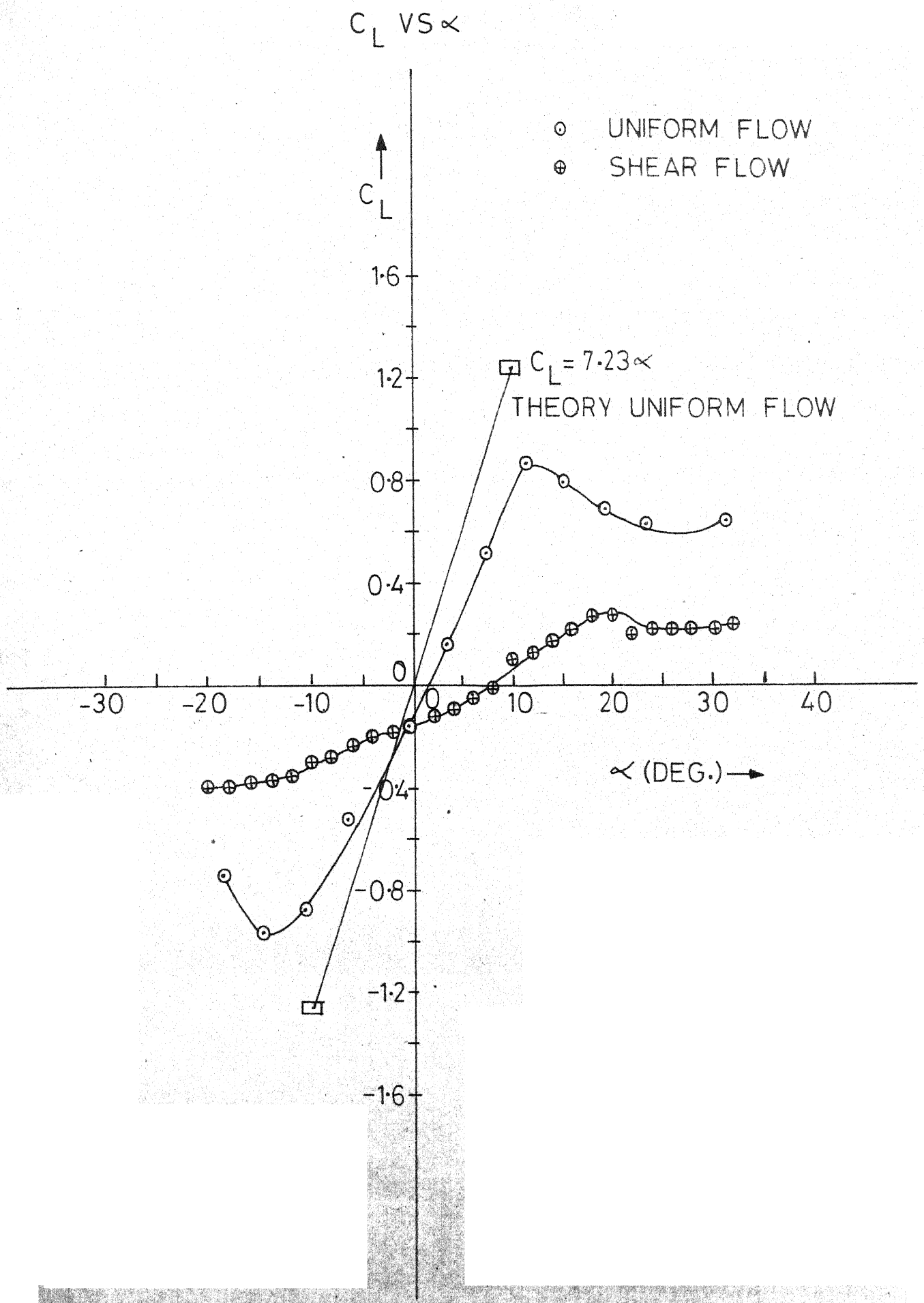

FIG. 11- SYMMETRIC AIRFOIL IN UNIFORM FLOW AND SHEAR FLOW (y=0)

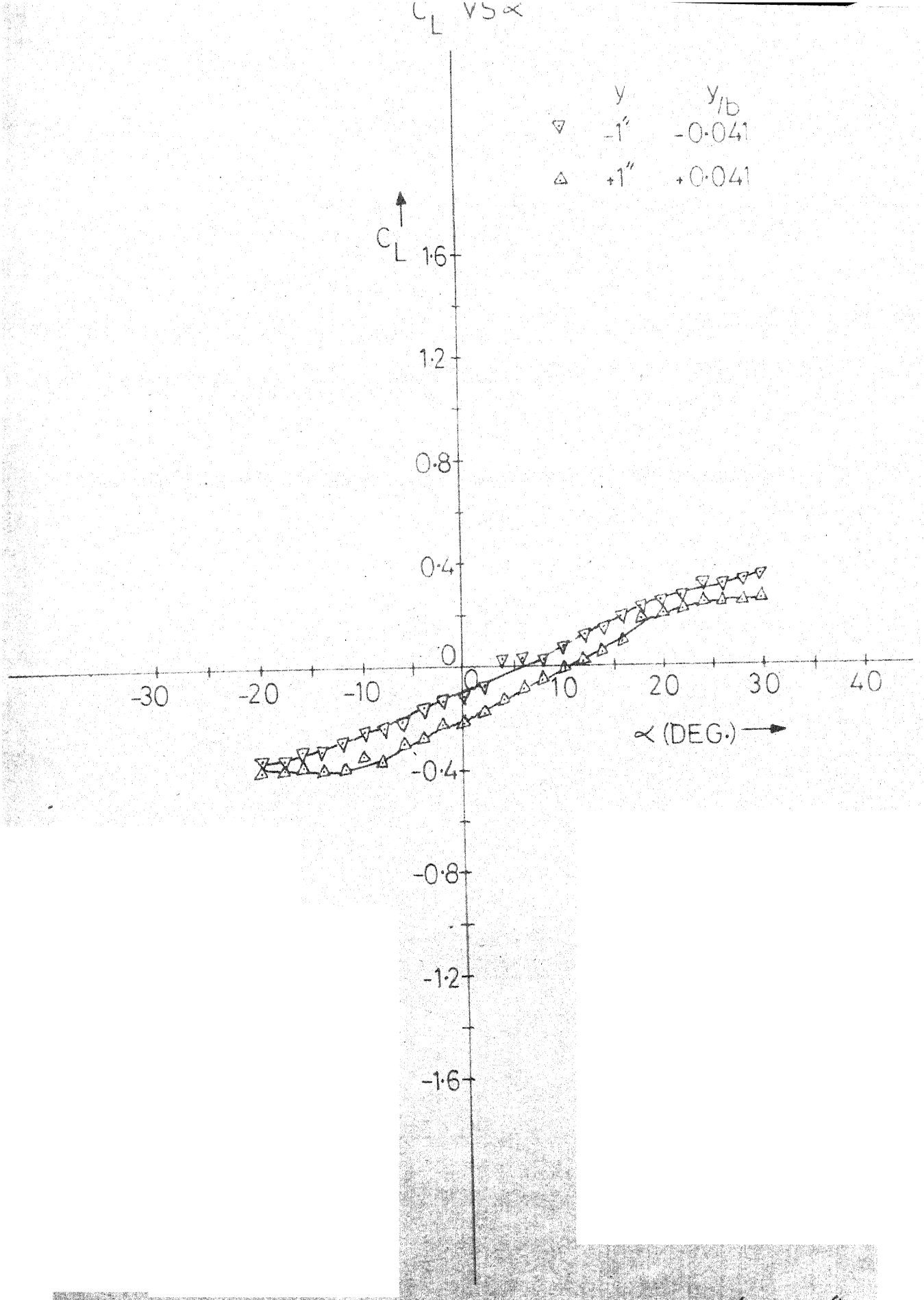

FIG. 12 – SYMMETRIC AIRFOIL IN SHEAR FLOW; y = +1", y = -1"

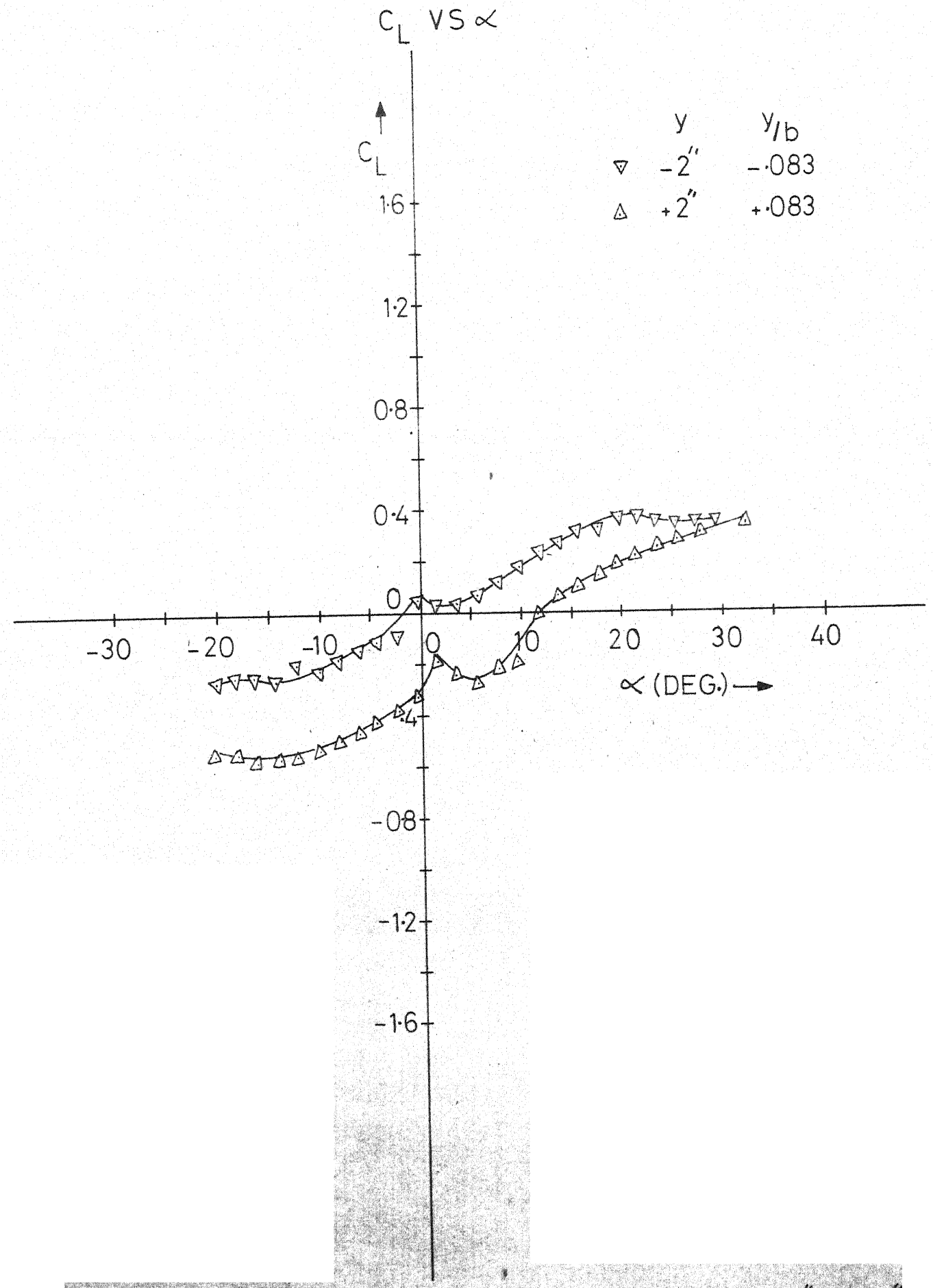

FIG. 13 – SYMMETRIC AIRFOIL IN SHEAR FLOW; $y = +2'', y = -2''$

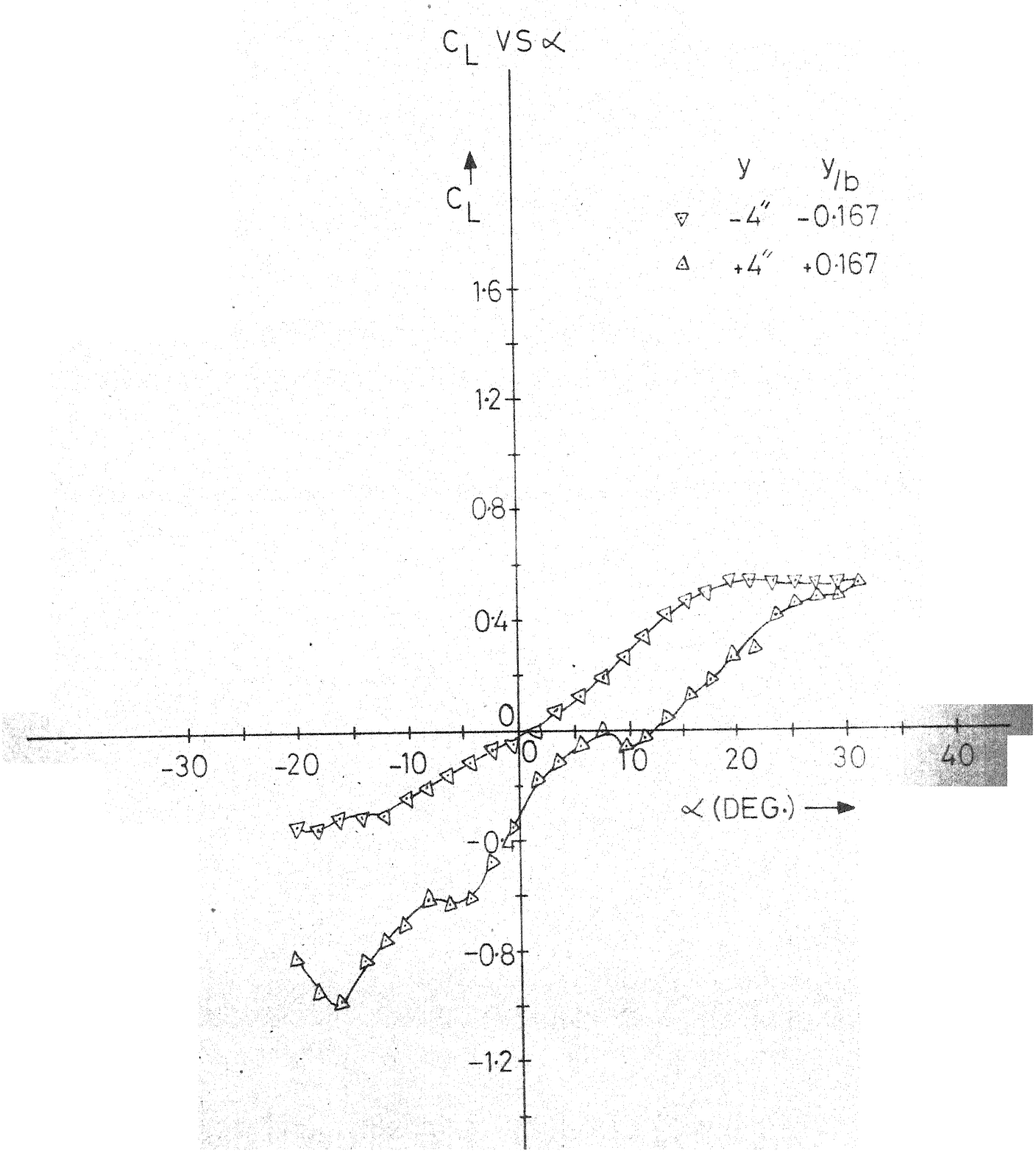
C_L VS α
C_L
y
$y_{/b}$
-4″
-0·167
+4″
+0·167
1·6
1·2
0·8
0·4
0
-0·4
-0·8
-1·2
-30
-20
-10
0
10
20
30
40
α (DEG·)

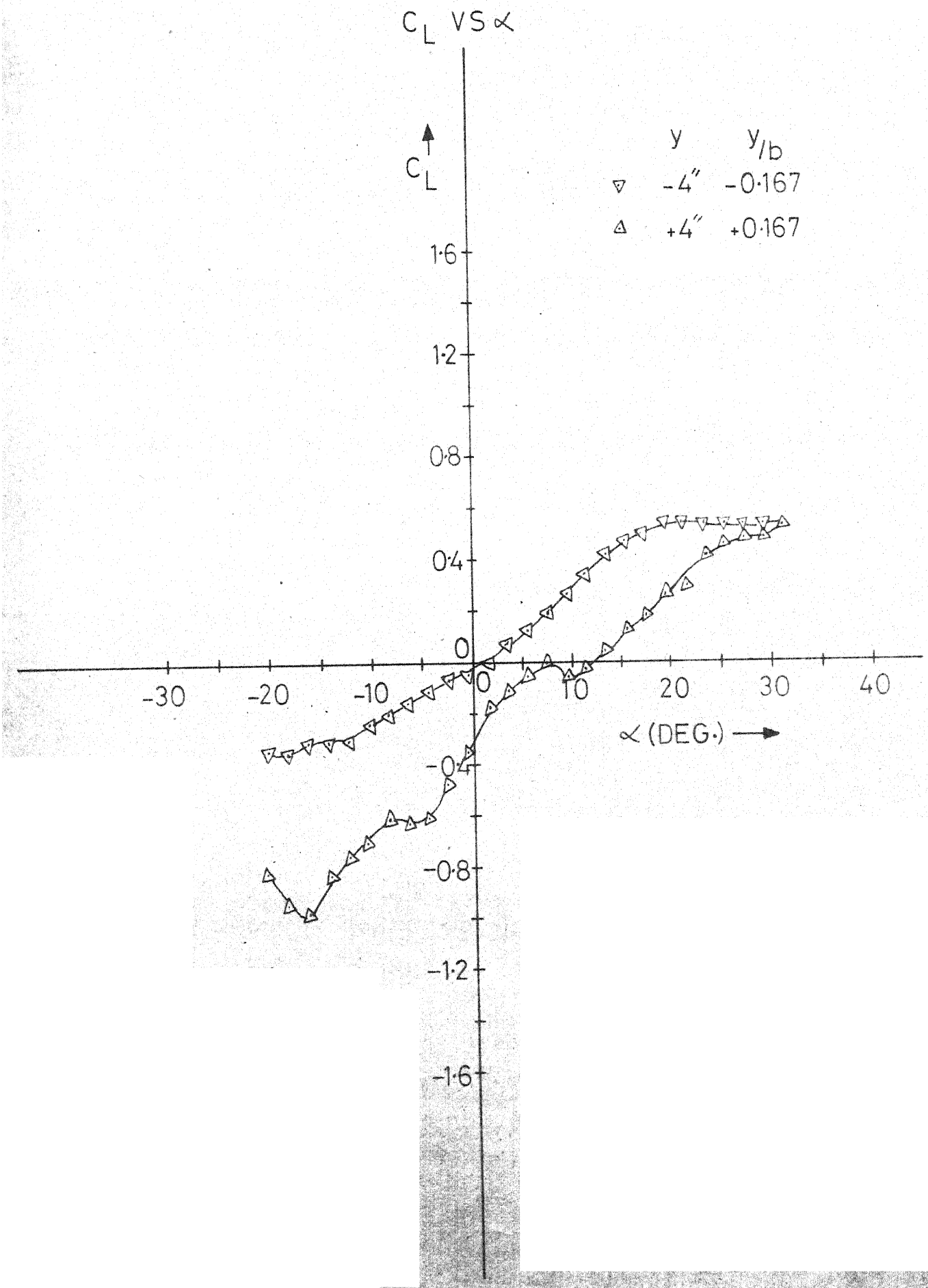

FIG. 14 – SYMMETRIC AIRFOIL IN SHEAR FLOW; y = +4″, y = – 4″

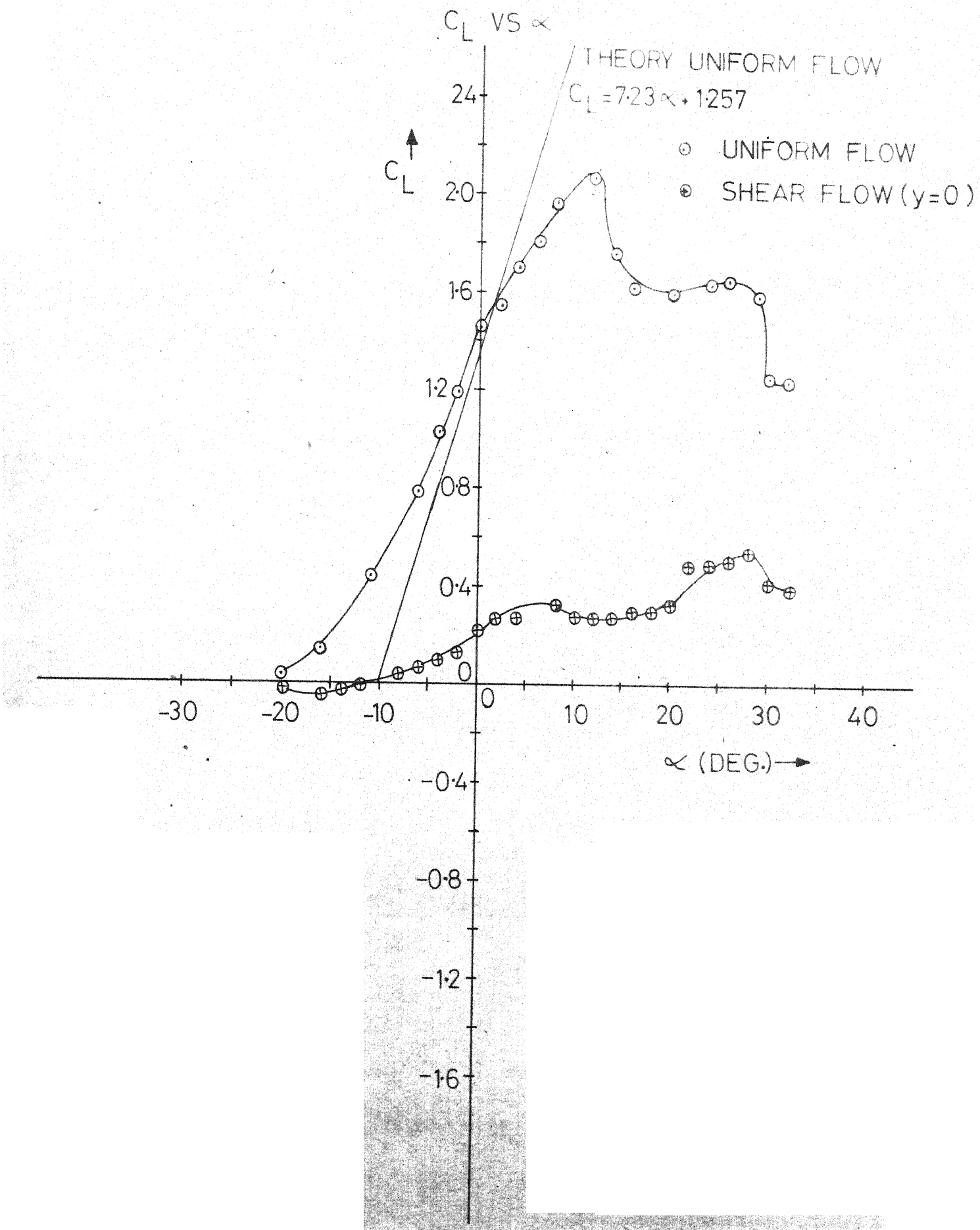

FIG. 15 – CAMBERED AIRFOIL IN UNIFORM FLOW AND SHEAR FLOW (y = 0)

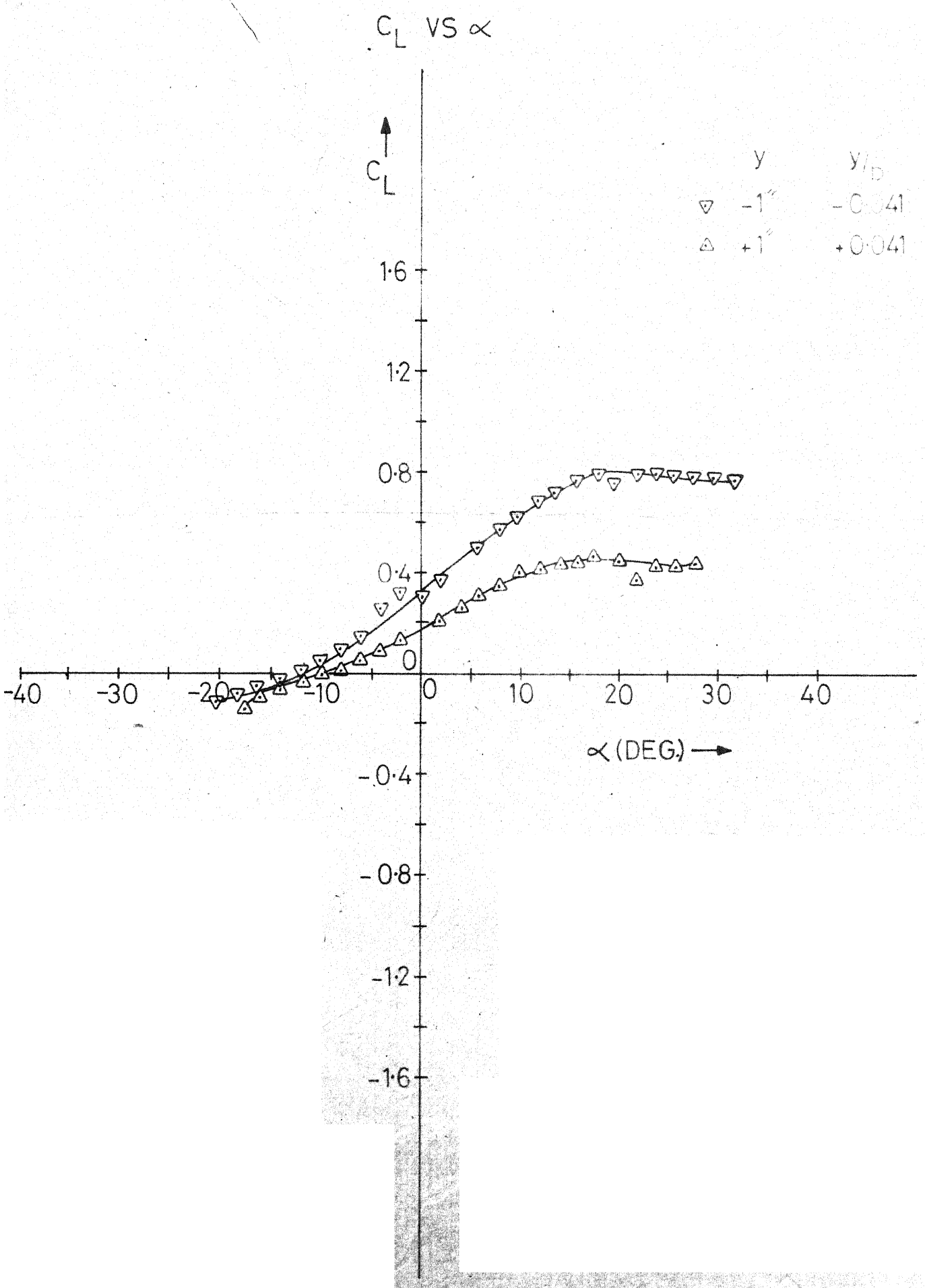

FIG. 16 – CAMBERED AIRFOIL IN SHEAR FLOW; y = +1", y = -1"

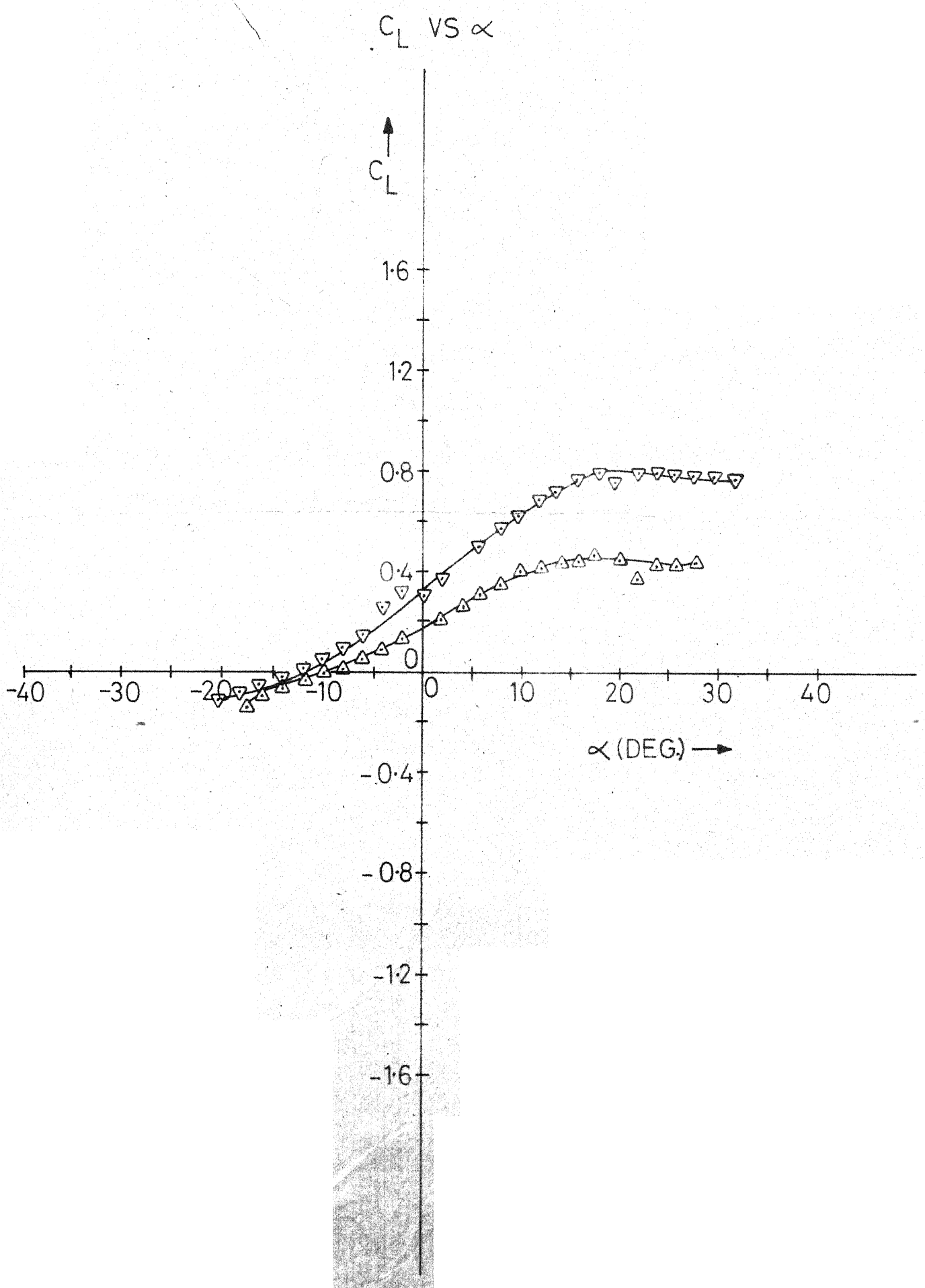

FIG. 16 – CAMBERED AIRFOIL IN SHEAR FLOW; $y = +1''$, $y = -1''$

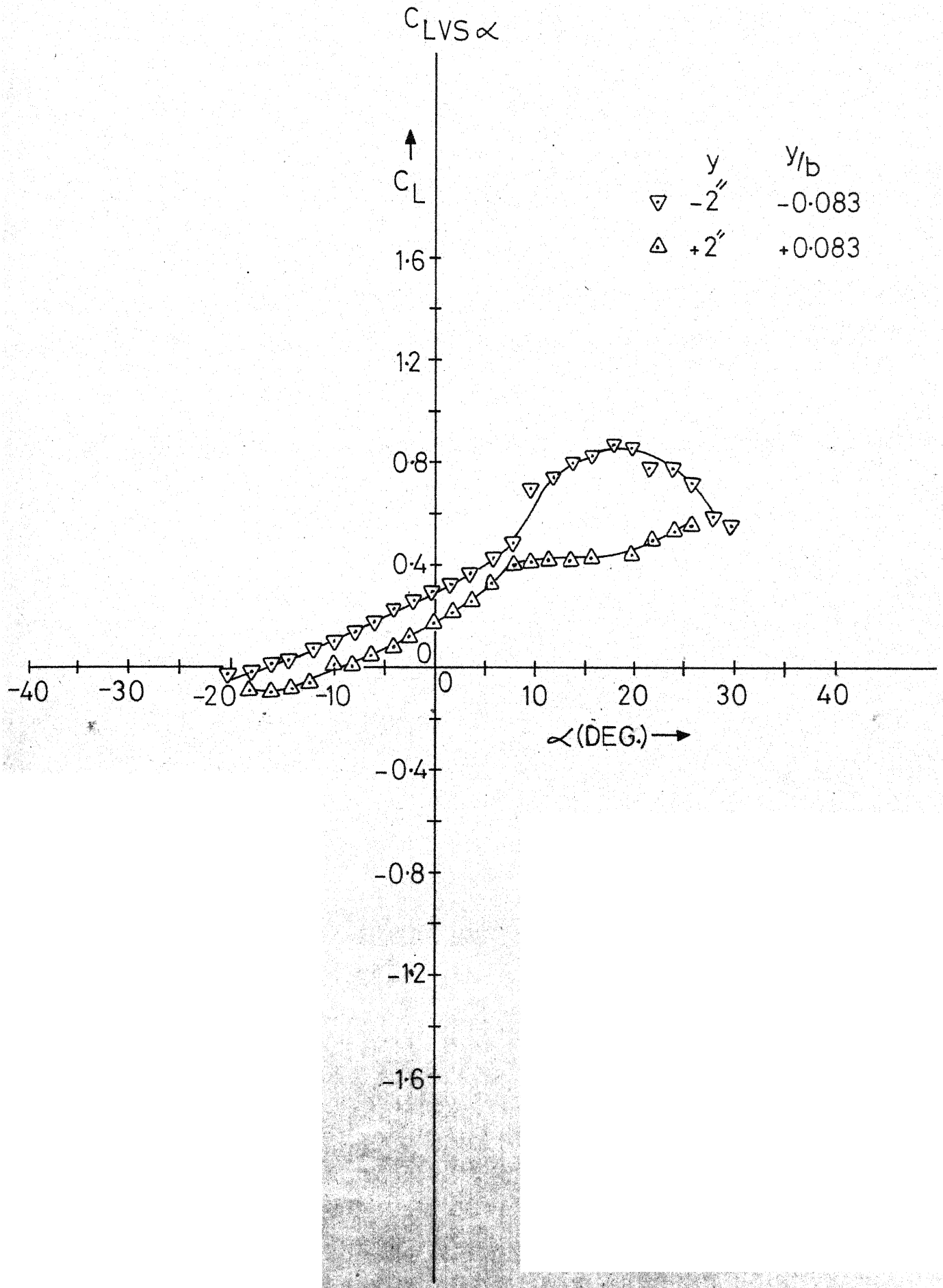

FIG. 17- CAMBERED AIRFOIL IN SHEAR FLOW; $y = +2''$, $y = -2''$

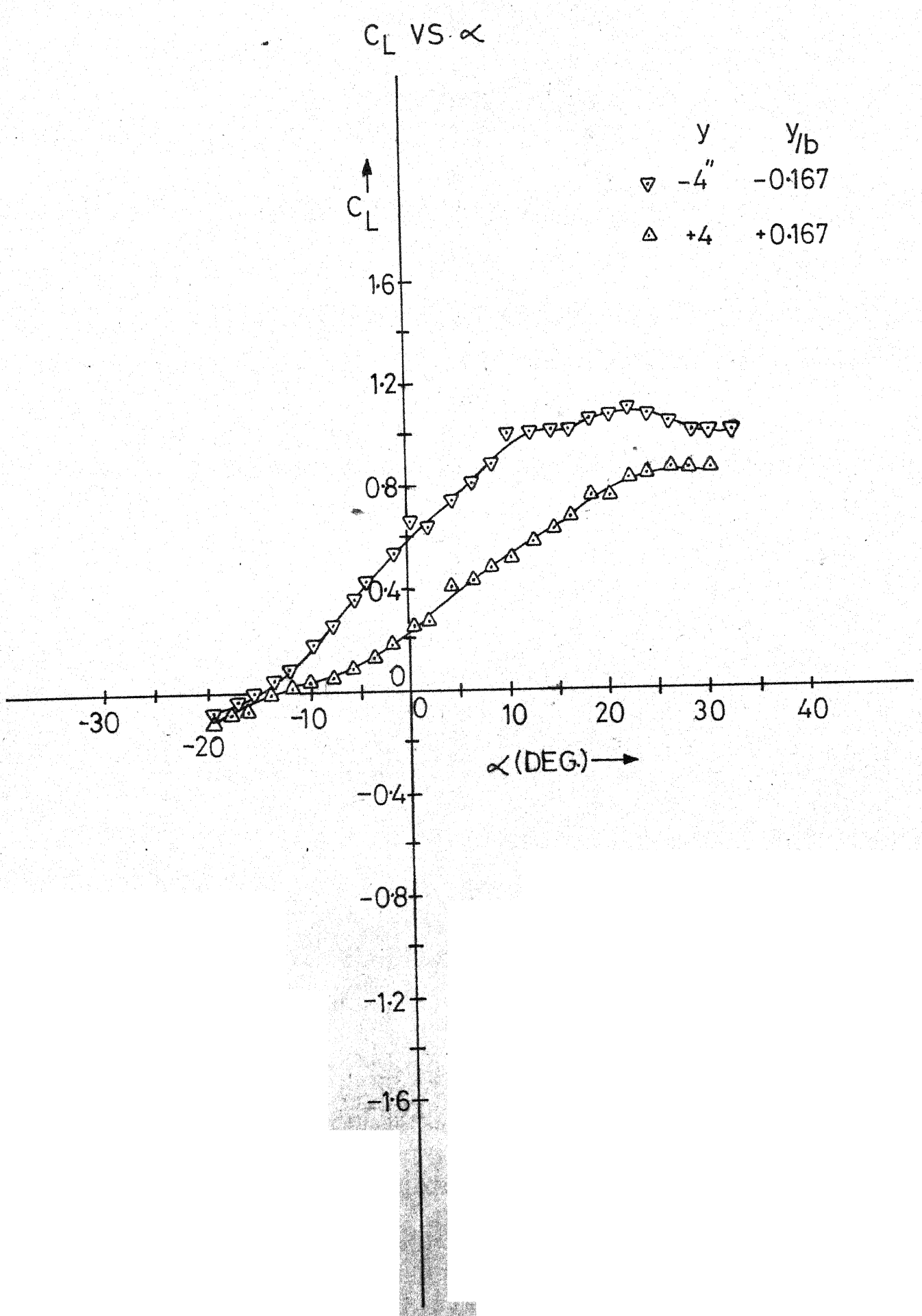

FIG. 18 - CAMBERED AIRFOIL IN SHEAR FLOW; y = +4", y = +4"

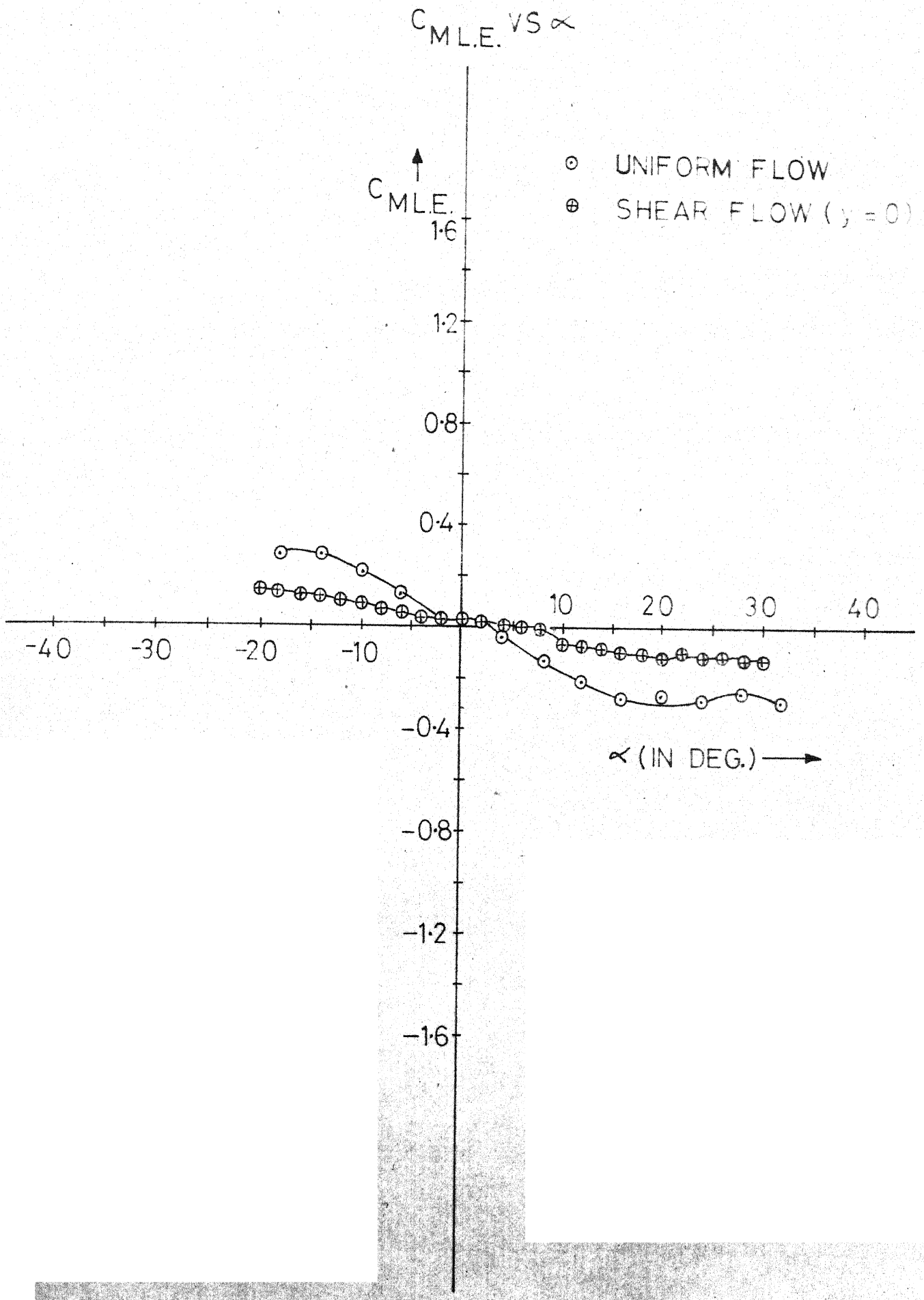

FIG 19. - SYMMETRIC AIRFOIL IN UNIFORM FLOW AND SHEAR FLOW (y = 0)

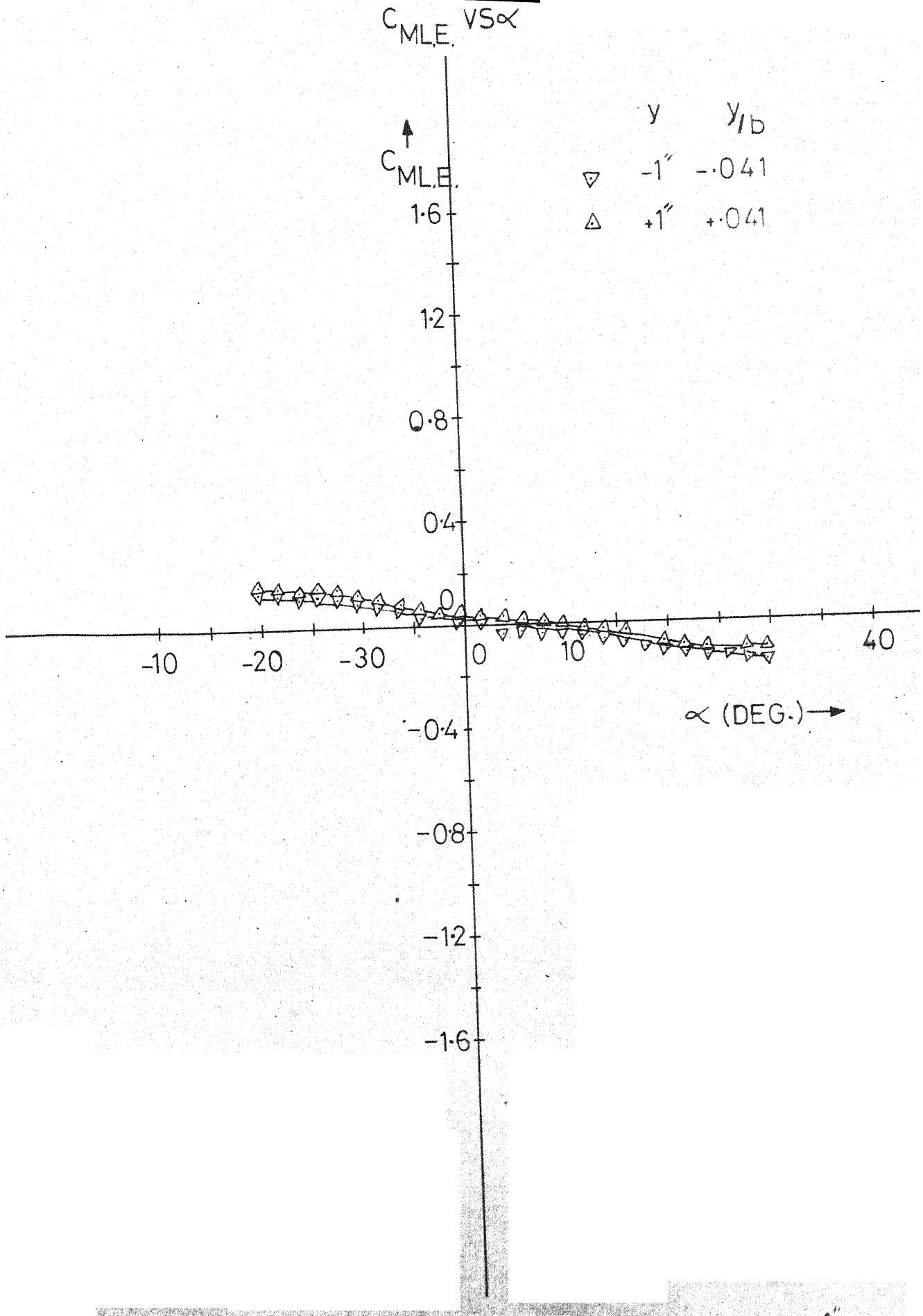

IG. 20- SYMMETRIC AIRFOIL IN SHEAR FLOW; y = +1", y =-

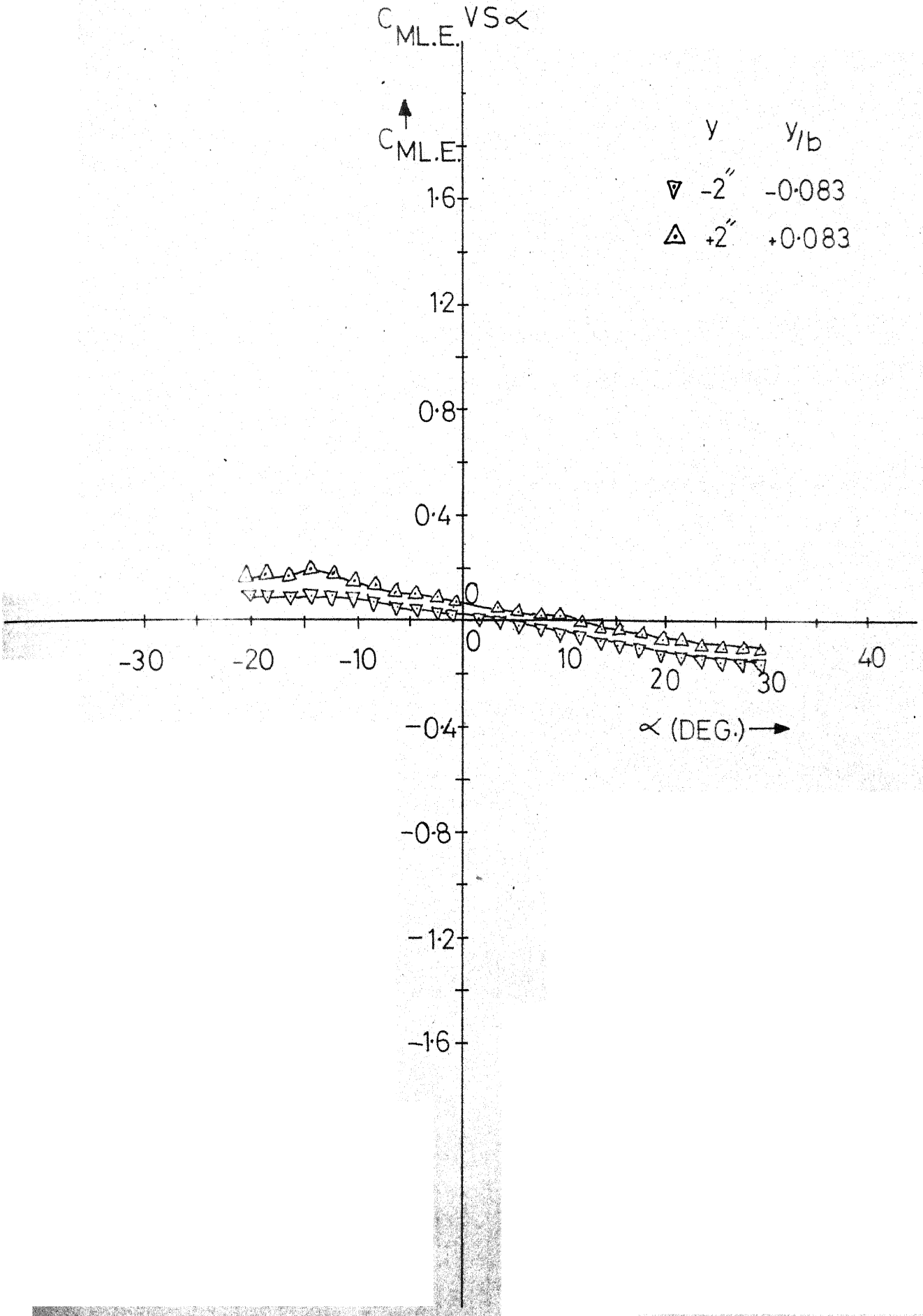

FIG. 21- SYMMETRIC AIRFOIL IN SHEAR FLOW; y = +2", y = -2"

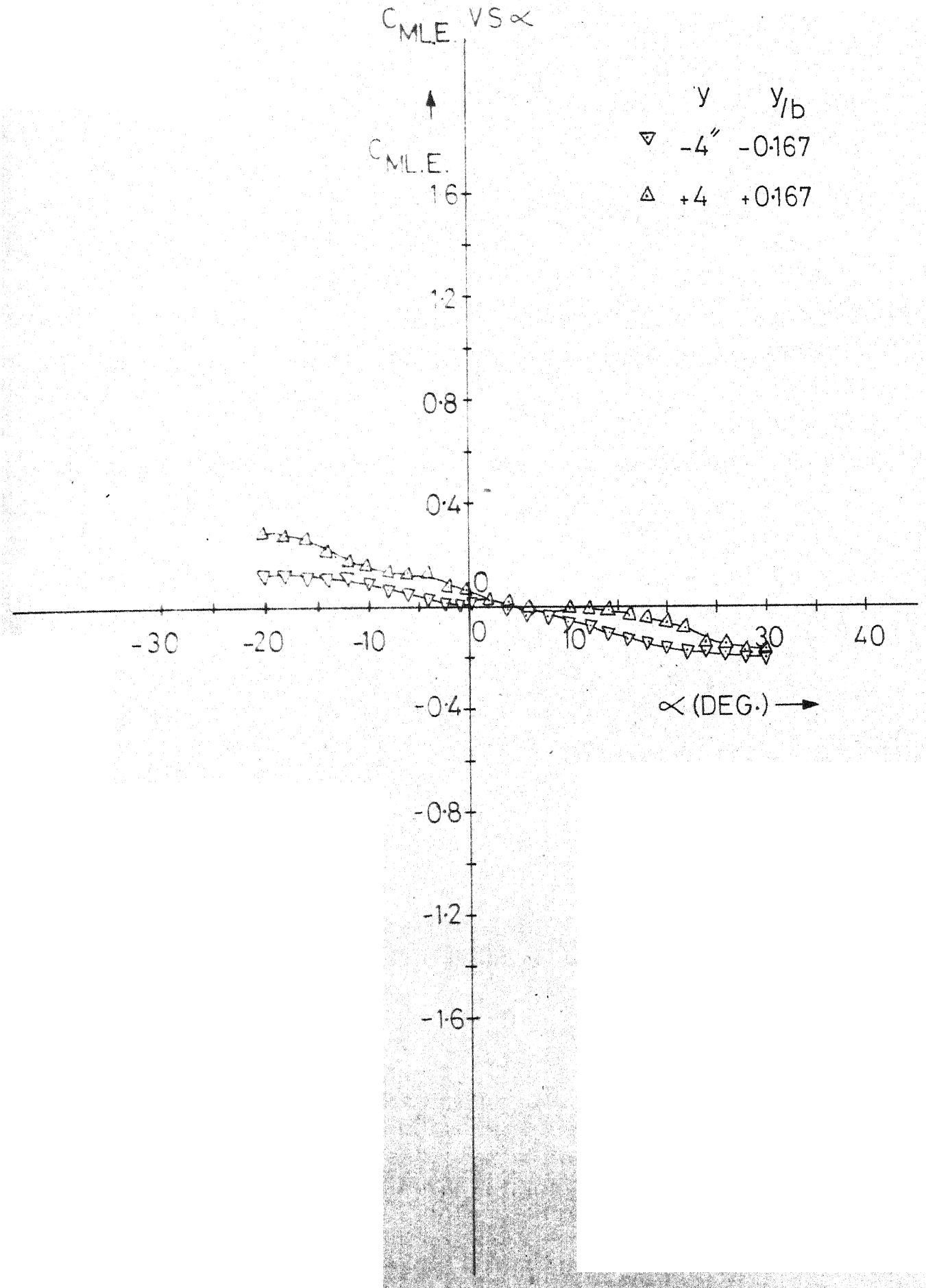

FIG. 22 - SYMMETRIC AIRFOIL IN SHEAR FLOW; y = + 4″, y = - 4″

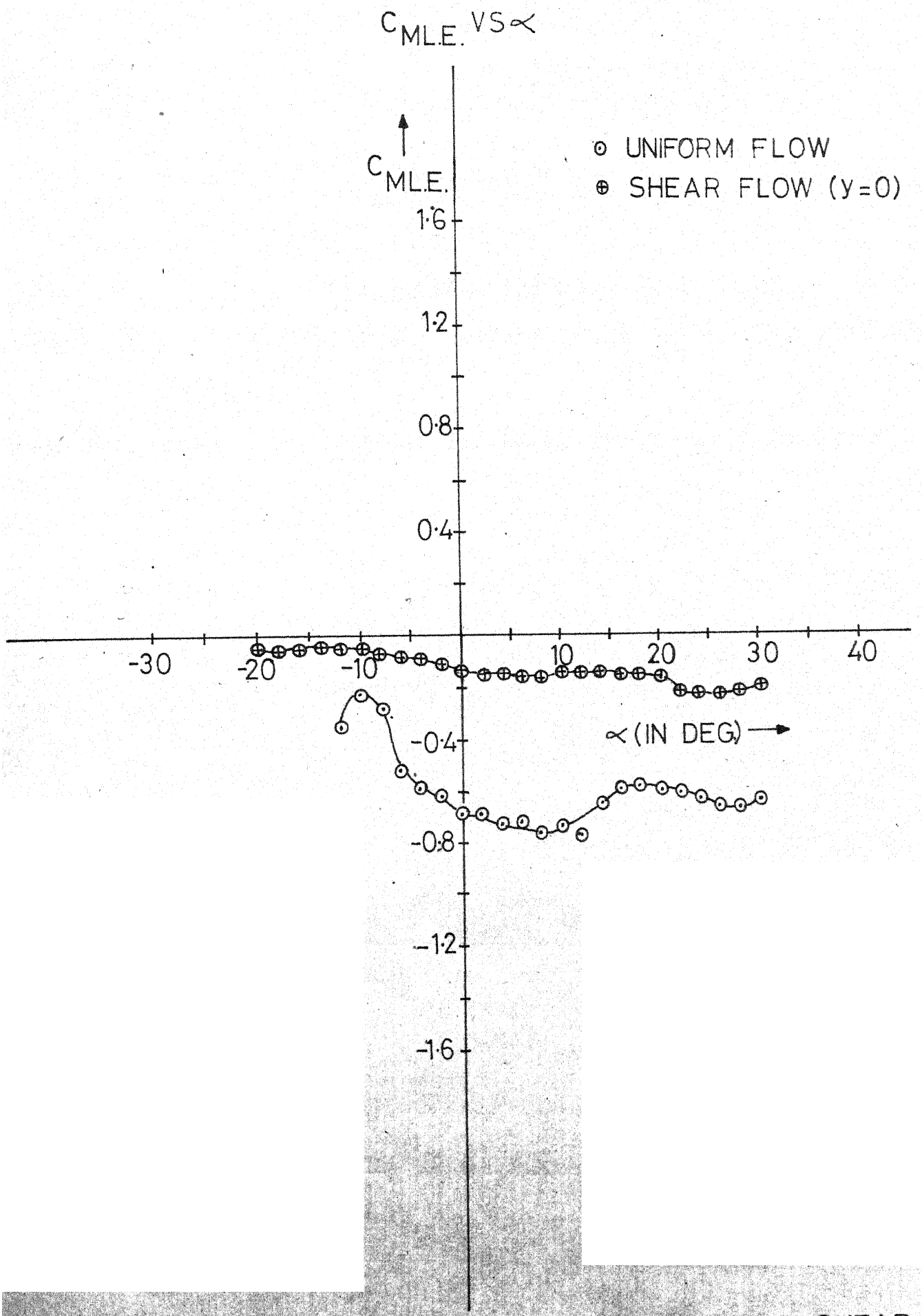

FIG.23 - CAMBERED AIRFOIL IN UNIFORM FLOW AND SHEAR FLOW (y= 0)

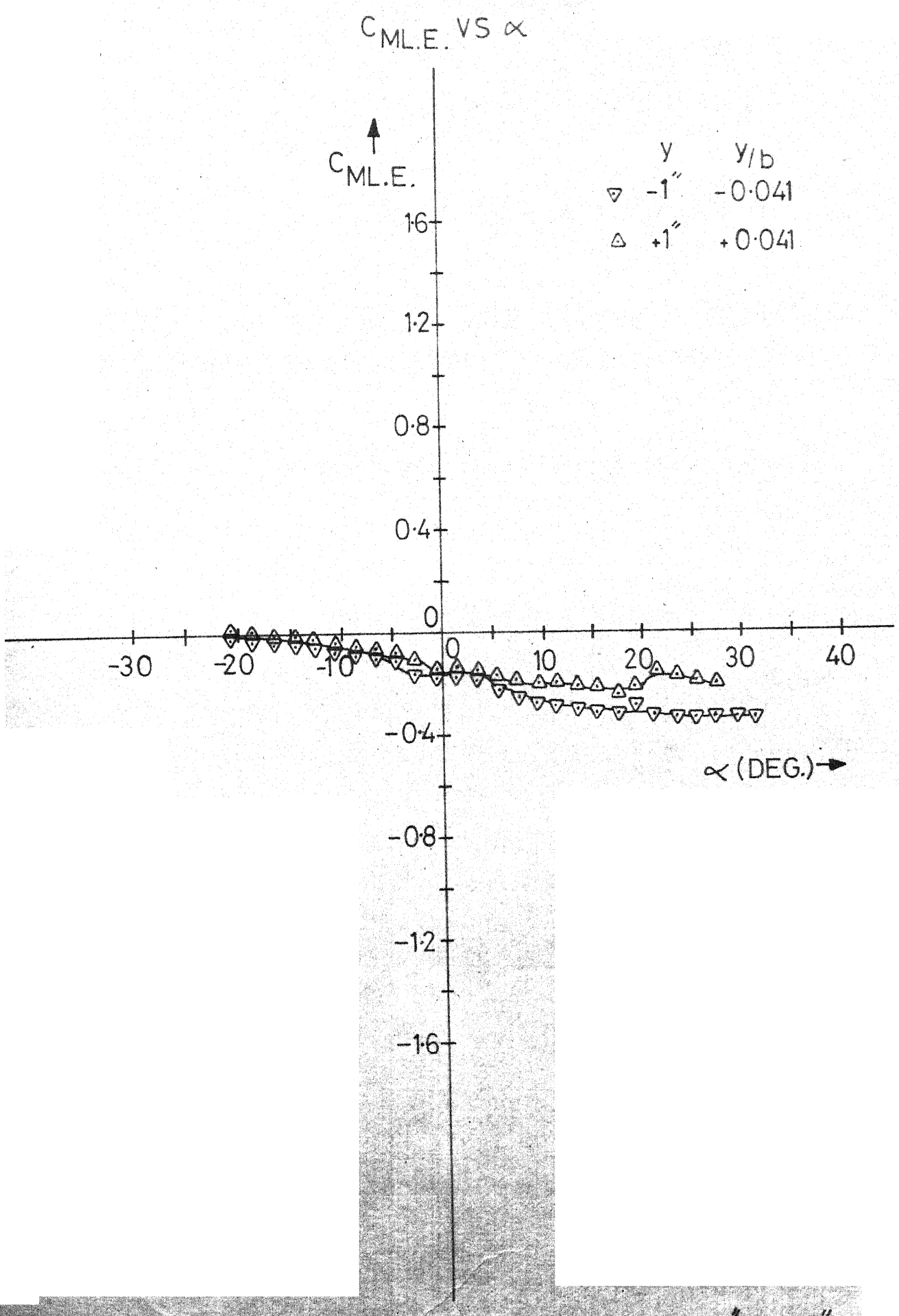

FIG. 24 – CAMBERED AIRFOIL IN SHEAR FLOW; y = +1", y = -1"

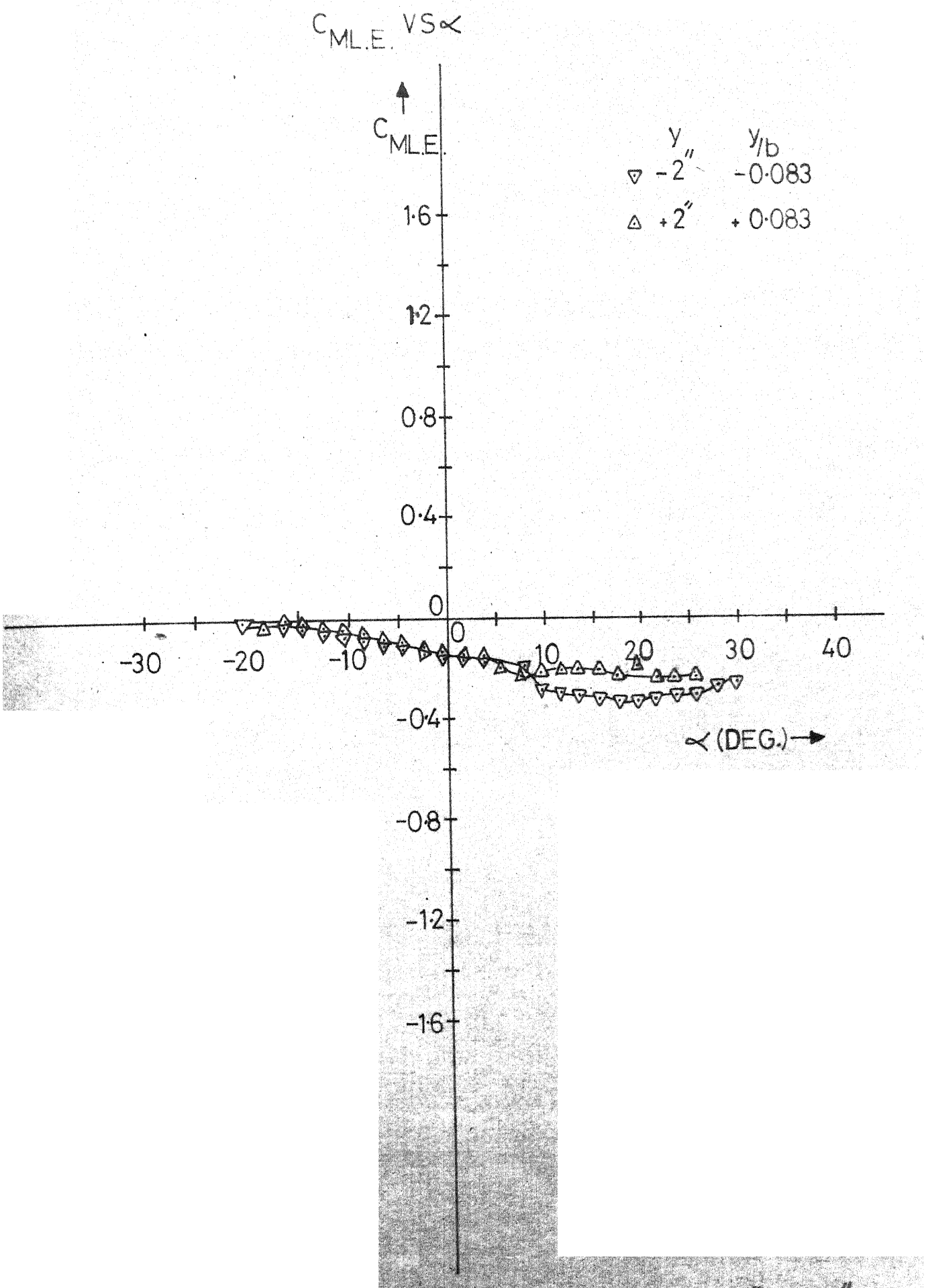

FIG. 25 – CAMBERED AIRFOIL IN SHEAR FLOW; $y = +2''$, $y = -2''$

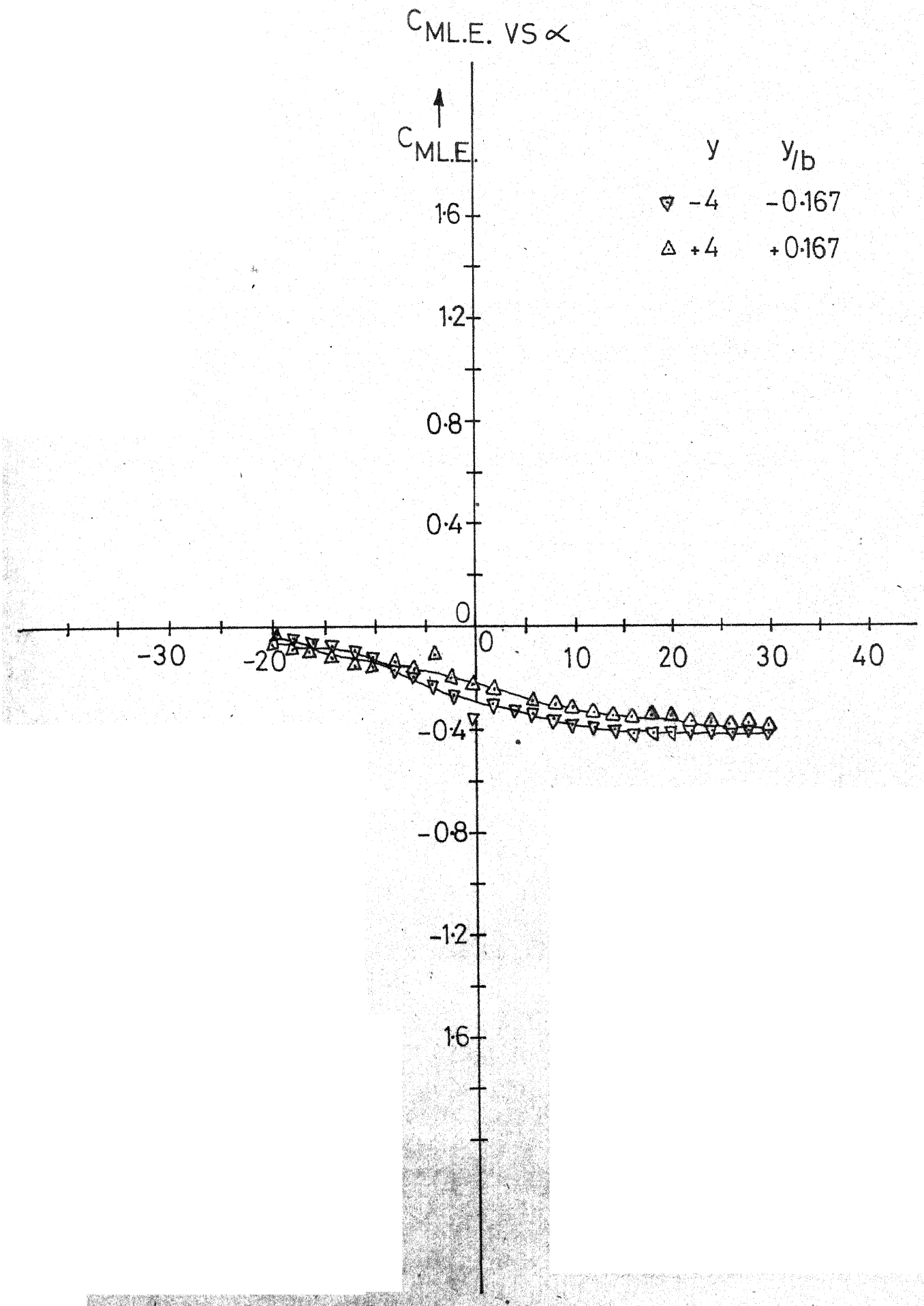

FIG.26 – CAMBERED AIRFOIL IN SHEAR FLOW; y = +4", y = -4"

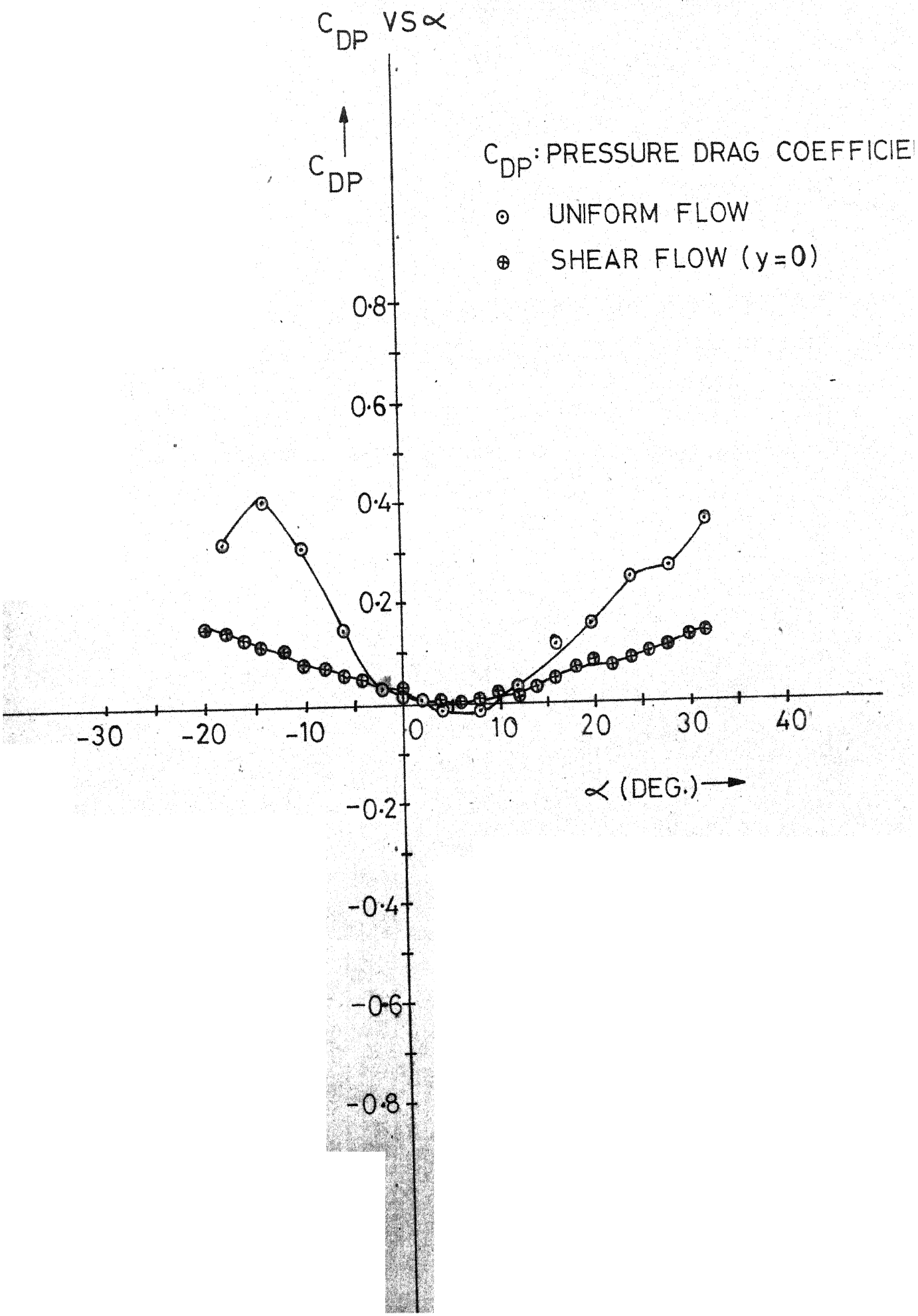
C_{DP} VS α
C_{DP}
C_{DP}: PRESSURE DRAG COEFFICIE
⊙ UNIFORM FLOW
⊕ SHEAR FLOW (y=0)
0·8
0·6
0·4
0·2
-0·2
-0·4
-0·6
-0·8
-30
-20
-10
0
10
20
30
40
α (DEG.)

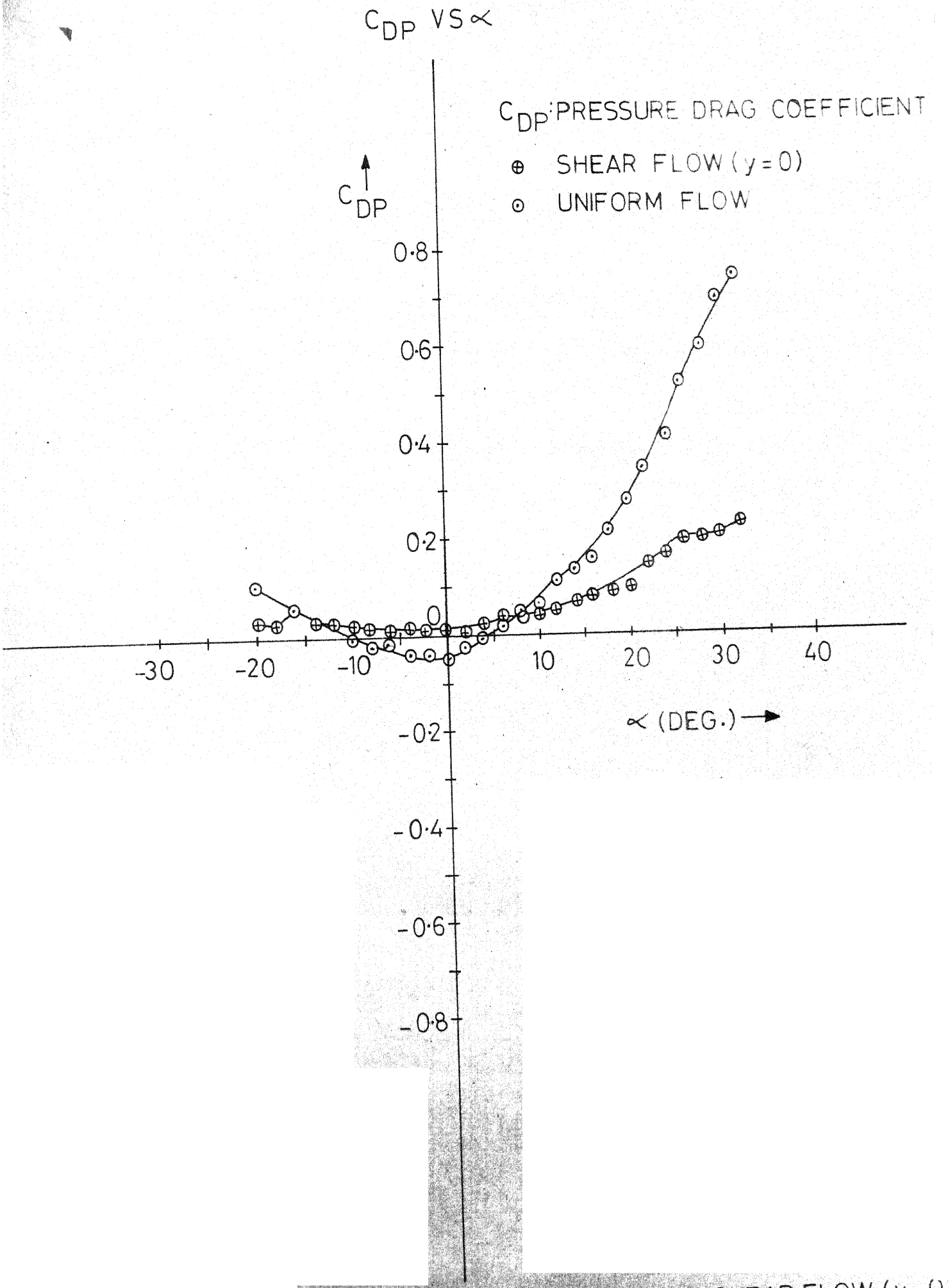

FIG. 28 – CAMBERED AIRFOIL IN UNIFORM FLOW AND SHEAR FLOW (y = 0

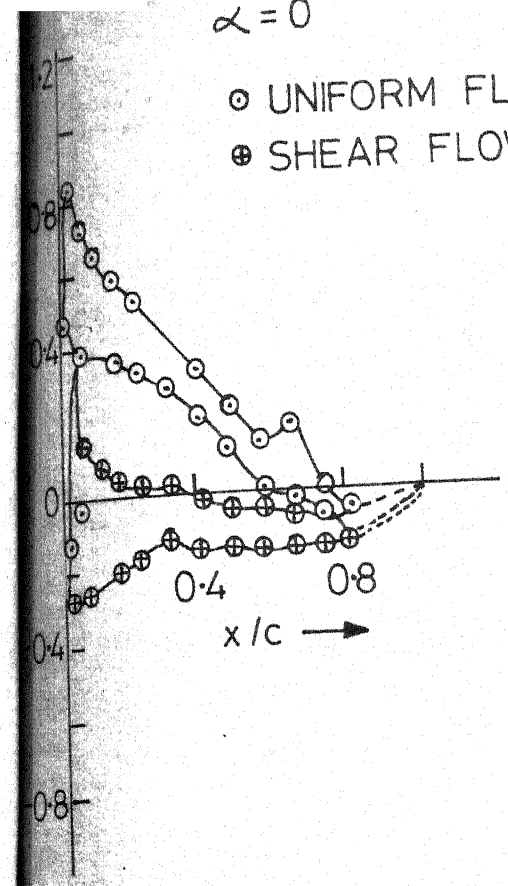

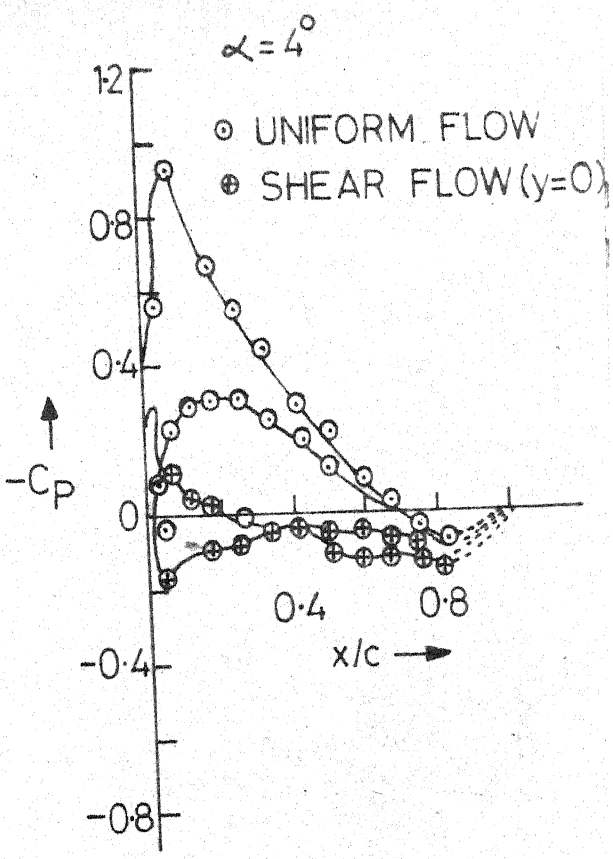

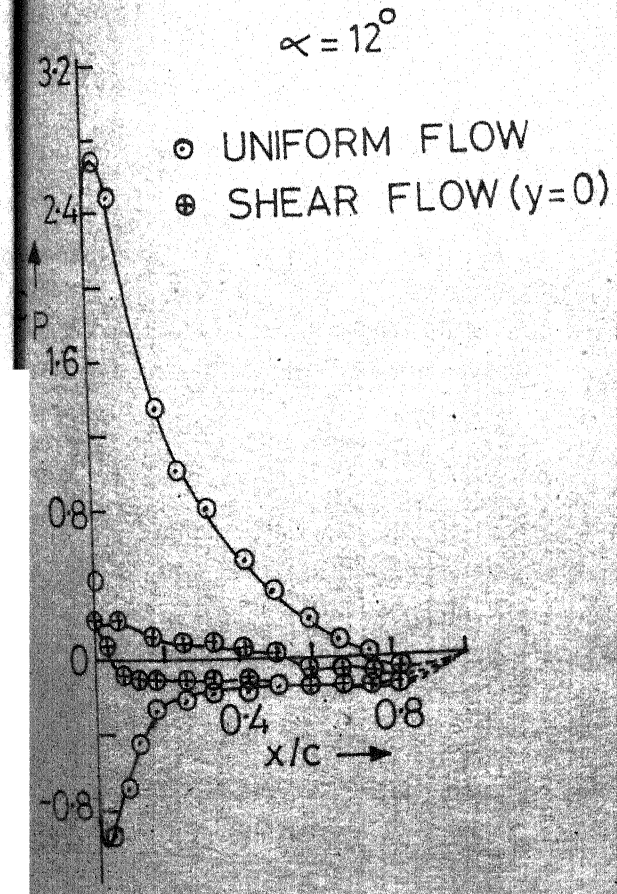

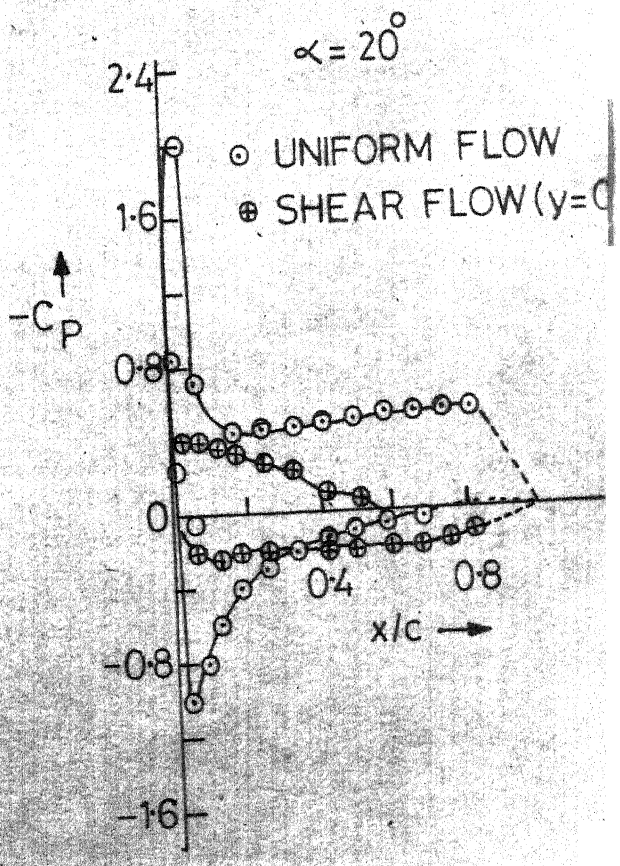

FIG. 29 – SYMMETRIC AIRFOIL IN UNIFORM FLOW AND SHEAR FLOW (y=0

$-C_P$ VS X/C

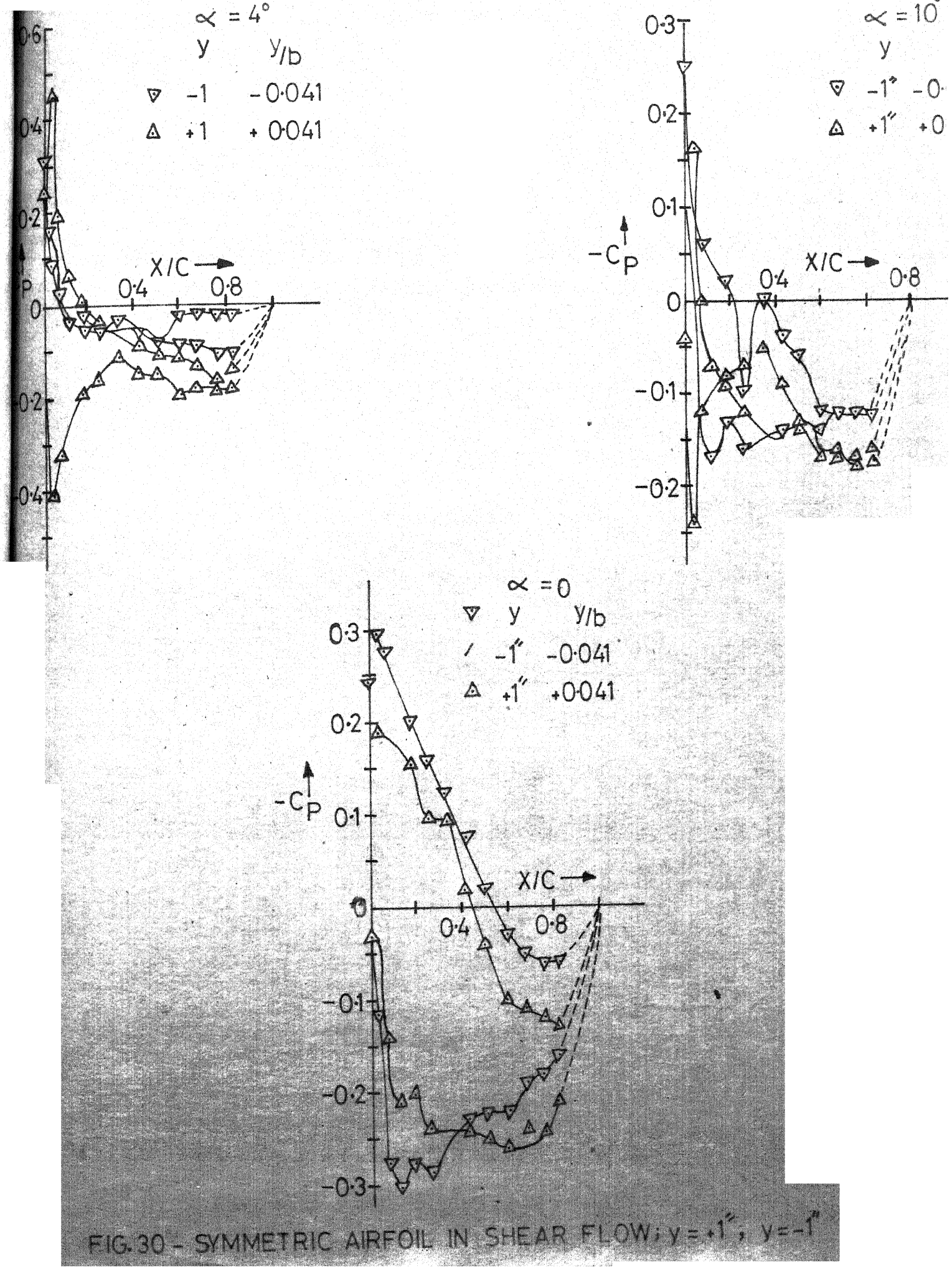

FIG. 30 – SYMMETRIC AIRFOIL IN SHEAR FLOW; $y = +1''$, $y = -1''$

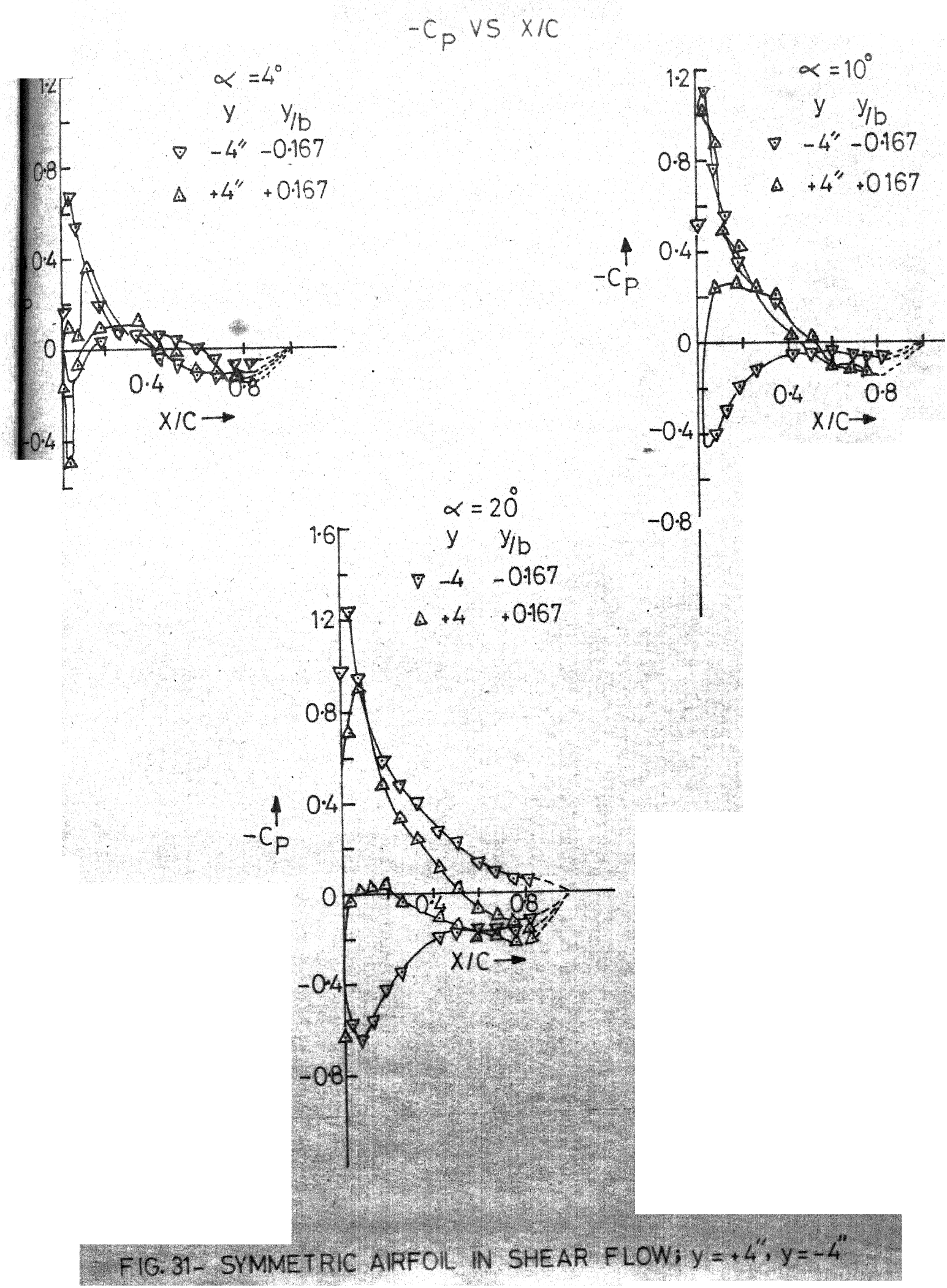

FIG. 31- SYMMETRIC AIRFOIL IN SHEAR FLOW; y = +4″, y = −4″

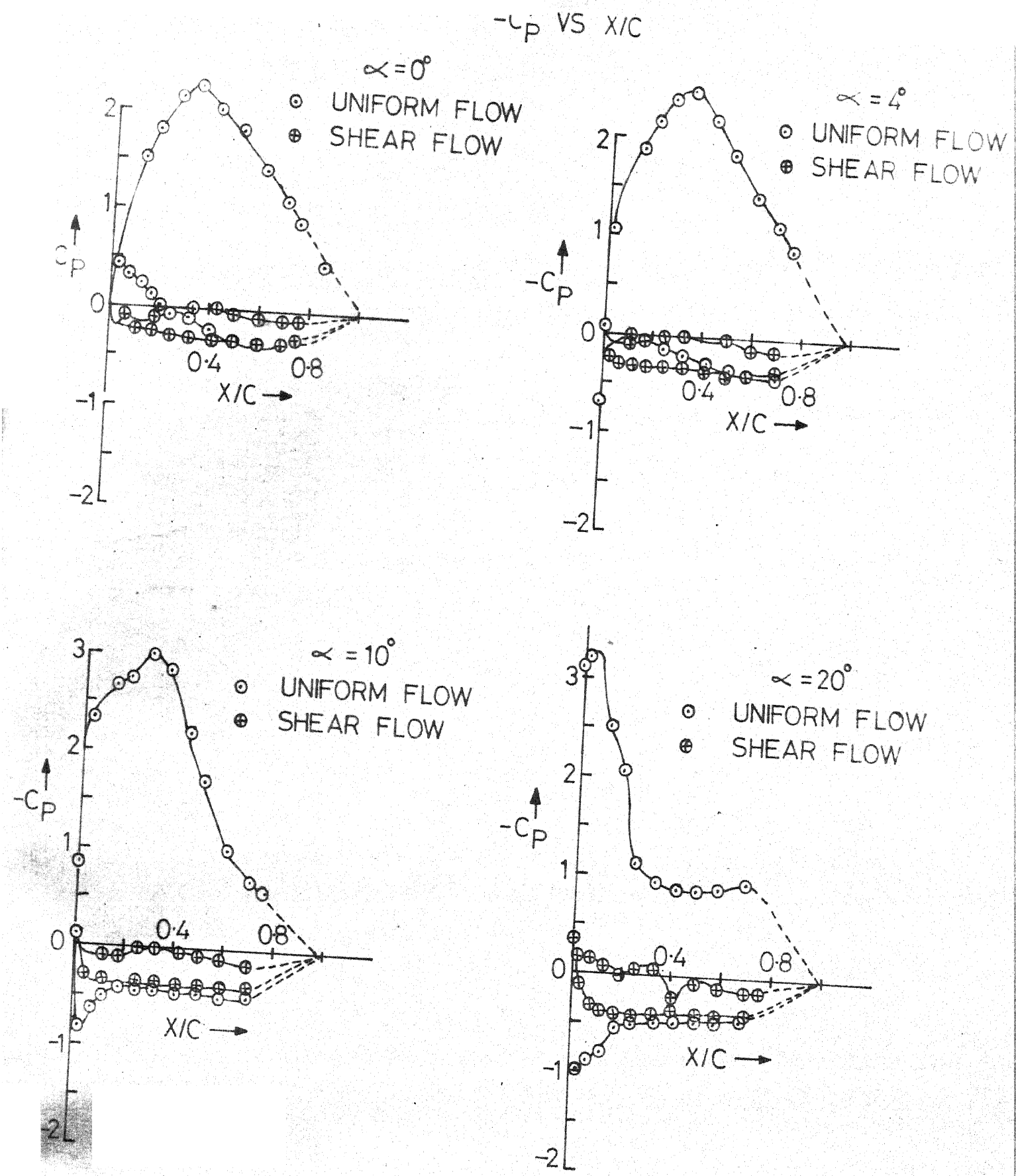

FIG. 32 - CAMBERED AIRFOIL IN UNIFORM FLOW AND SHEAR FLOW (y=0).

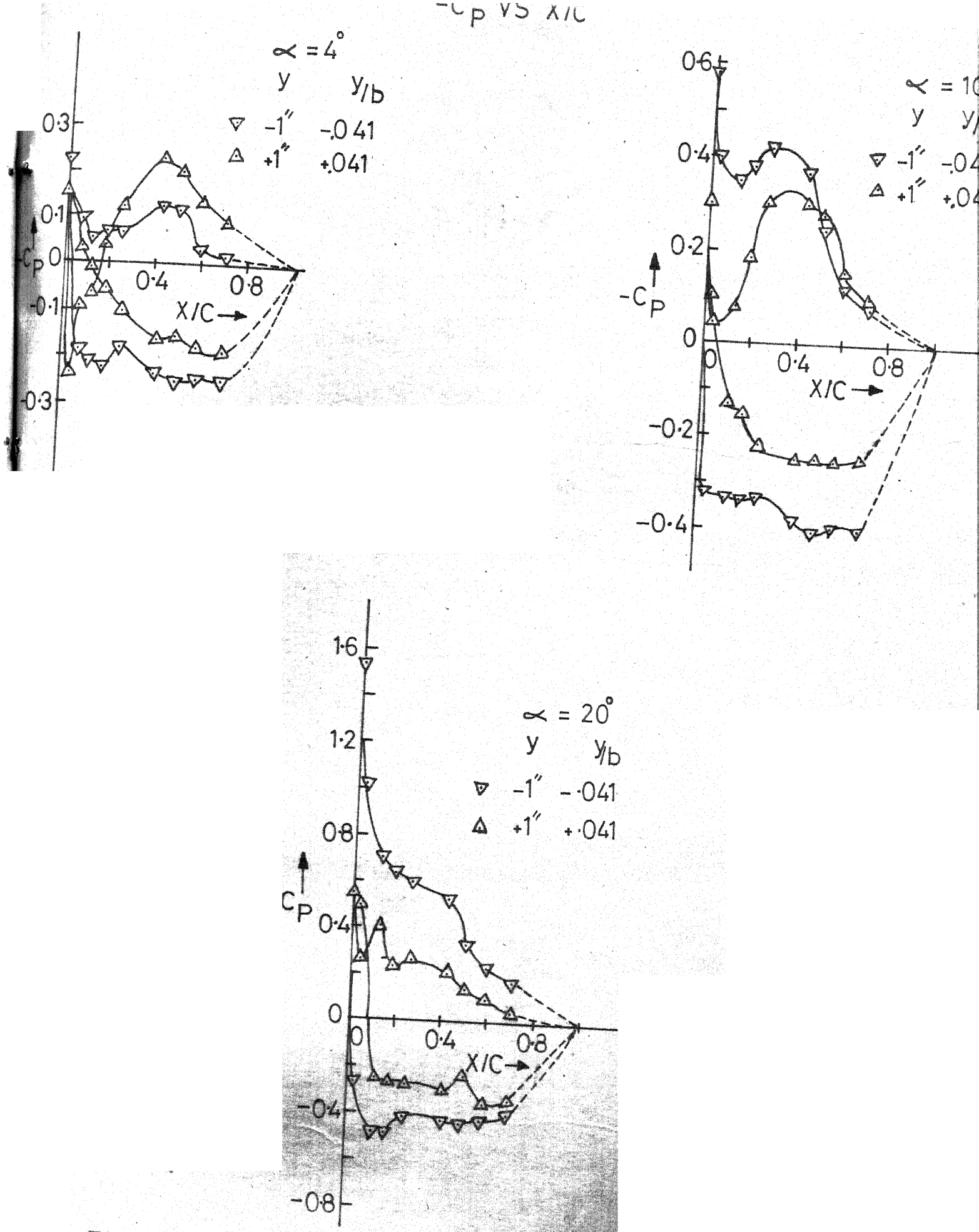

FIG. 33 - CAMBERED AIRFOIL IN SHEAR FLOW; y = +1″, y = -1″

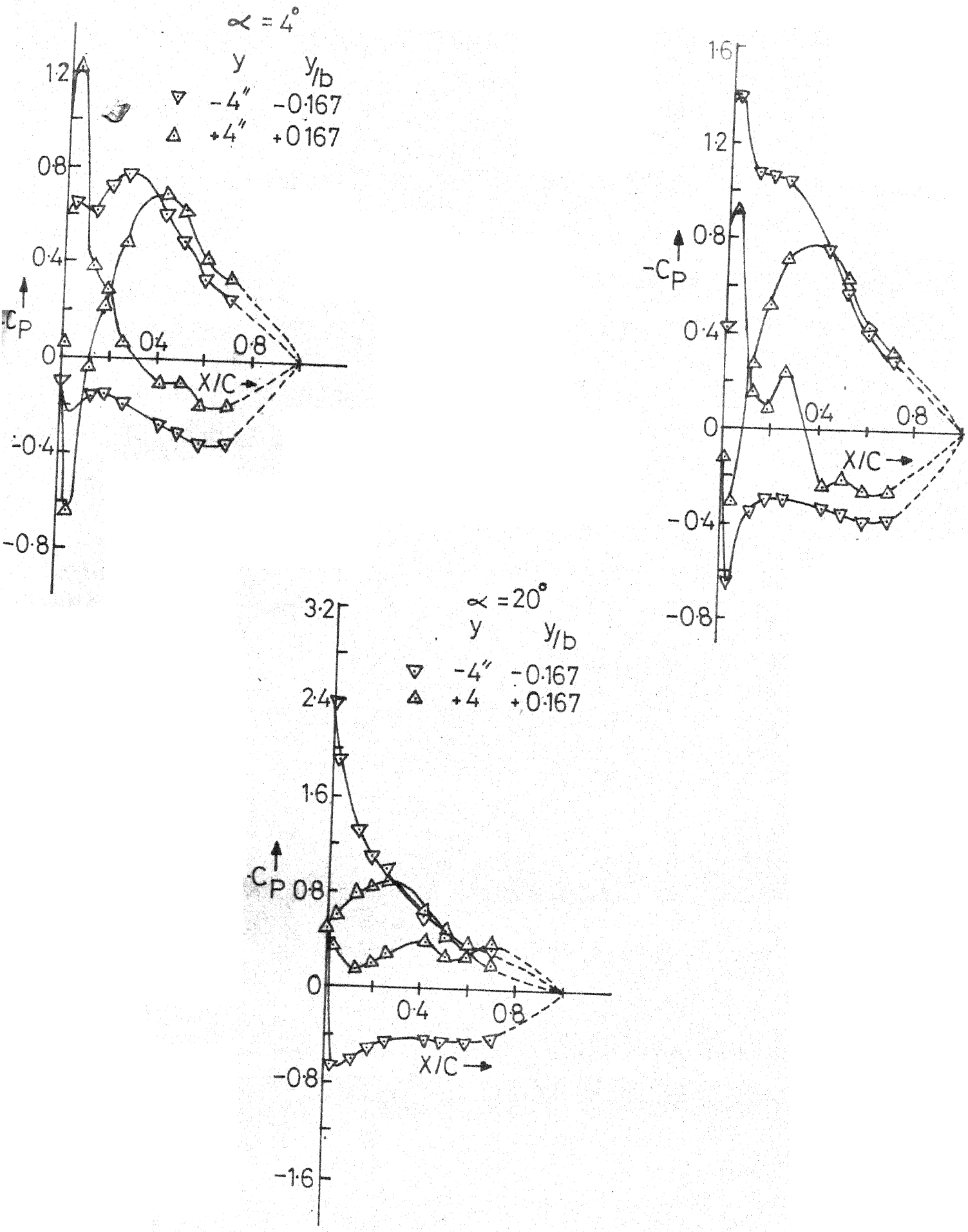

34 - CAMBERED AIRFOIL AND SHEAR FLOW, y = +4", y = −4"

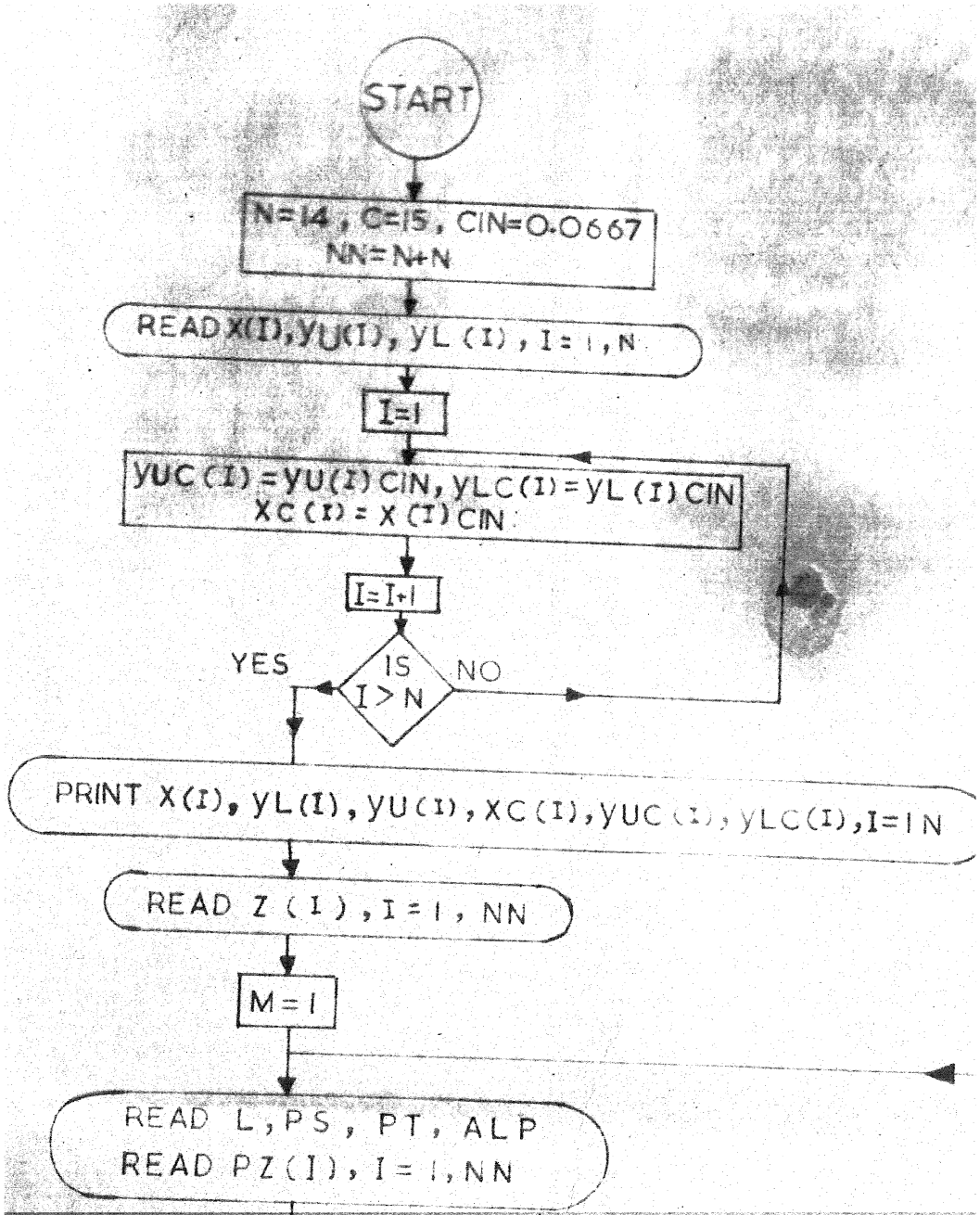
START
N=14, C=15, CIN=0.0667
NN=N+N
READ X(I), YU(I), YL(I), I=1,N
I=1
YUC(I)=YU(I)CIN, YLC(I)=YL(I)CIN
XC(I)=X(I)CIN
I=I+1
IS I>N
YES
NO
PRINT X(I), YL(I), YU(I), XC(I), YUC(I), YLC(I), I=1N
READ Z(I), I=1, NN
M=1
READ L, PS, PT, ALP
READ PZ(I), I=1, NN